Contributions of Trans-boundary Transport to Summertime Air Quality in Beijing, China

Jiarui Wu[1,3], Guohui Li[1*], Junji Cao[1*], Naifang Bei[2], Yichen Wang[1], Tian Feng[1, 2], Rujin Huang[1], Suixin Liu[1], Qiang Zhang[4], and Xuexi Tie[1]

[1]Key Lab of Aerosol Chemistry and Physics, SKLLQG, Institute of Earth Environment, Chinese Academy of Sciences, Xi'an, China
[2]School of Human Settlements and Civil Engineering, Xi'an Jiaotong University, Xi'an, Shaanxi, China
[3]University of Chinese Academy of Science, Beijing, China
[4]Department of Environmental Sciences and Engineering, Tsinghua University, Beijing, China
[*]Correspondence to: Guohui Li (ligh@ieecas.cn) and Junji Cao (jjcao@ieecas.cn)

Abstract: In the present study, the WRF-CHEM model is used to evaluate the contributions of trans-boundary transport to the air quality in Beijing during a persistent air pollution episode from 5 to 14 July 2015 in Beijing-Tianjin-Hebei (BTH), China. Generally, the predicted temporal variations and spatial distributions of $PM_{2.5}$ (fine particulate matter), O_3 (ozone), and NO_2 are in good agreement with observations in BTH. The WRF-CHEM model also reproduces reasonably well the temporal variations of aerosol species compared to measurements in Beijing. The factor separation approach is employed to evaluate the contributions of trans-boundary transport of non-Beijing emissions to the $PM_{2.5}$ and O_3 levels in Beijing. On average, in the afternoon during the simulation episode, the local emissions contribute 22.4% to the O_3 level in Beijing, less than 36.6% from non-Beijing emissions. The O_3 concentrations in Beijing are decreased by 5.1% in the afternoon due to interactions between local and non-Beijing emissions. The non-Beijing emissions play a dominant role in the $PM_{2.5}$ level in Beijing, with a contribution of 61.5%, much higher than 13.7% from Beijing local emissions. The emission interactions between local and non-Beijing emissions enhance the $PM_{2.5}$ concentrations in Beijing, with a contribution of 5.9%. Therefore, the air quality in Beijing is generally determined by the trans-boundary transport of non-Beijing emissions during summertime, showing that the cooperation with neighboring provinces to mitigate pollutant emissions is a key for Beijing to improve air quality.

1 Introduction

Beijing, the capital of China, has become an environmentally stressed city due to growing population, increasing transportation activity, and city expansion (Parrish and Zhu, 2009). Beijing is situated in northeastern China, surrounded from the southwest to the northeast by the Taihang Mountains and the Yanshan Mountains and open to the North China Plain (NCP) in the south and east. Unfortunately, NCP has become one of the most polluted areas in China due to rapid industrialization and urbanization (Zhang et al., 2013). When south or east winds are prevalent in NCP, air pollutants originated from NCP are transported to Beijing and surrounding areas and subject to be accumulated due to the mountain blocking, causing heavy air pollution in Beijing (Long et al., 2016).

$PM_{2.5}$ (fine particulate matter) and O_3 (ozone) are considered to be the most serious air pollutants of concern in Beijing during summertime (e.g., Xie et al., 2015; Zheng et al., 2015; Chen et al., 2015; Wang et al., 2016). The mean summertime $PM_{2.5}$ mass concentration is about 80 μg m^{-3} in 2013 (Li et al., 2015a), exceeding the second grade of National Ambient Air Quality Standards (NAAQS) in China and also higher than the average $PM_{2.5}$ concentration of 78.1 μg m^{-3} during the period from 2004 to 2012 (Liu et al., 2015). During haze pollution events in summer 2014, the $PM_{2.5}$ concentration generally reaches 100 μg m^{-3}, and even exceeds 150 μg m^{-3} in Beijing (Wang et al., 2016). An increasing O_3 trend has been observed in Beijing from 2002 to 2010 (Wang et al., 2012; Wang et al., 2013). The average maximum 1-h O_3 concentration has been reported to achieve 140 μg m^{-3} during summertime of 2013 in Beijing (Wang et al., 2014a). Wang et al. (2016) have demonstrated that the summertime O_3 mass concentration reached high levels in 2014 in Beijing, with a daily

54 average of up to 110 μg m^{-3}. Chen et al. (2015) have further shown that the average
55 maximum daily O_3 concentrations were higher than 150 μg m^{-3} during the summer in 2015 at
56 most of monitoring sites in Beijing.

57 In recent years, Beijing has implemented aggressive emission control strategies to
58 ameliorate the air quality (Parrish and Zhu, 2009). Both NO_x ($NO+NO_2$) and total VOCs
59 (volatile organic compounds) in Beijing have decreased linearly since 2002, while the
60 daytime average O_3 concentration still increased rapidly (Tang et al., 2009; Wang et al., 2012;
61 Zhang et al., 2014). Zhang et al. (2014) have highlighted the importance of the
62 trans-boundary transport and the cooperation with neighboring provinces to control the O_3
63 level in Beijing. Pollutants transported from outside of Beijing and formed locally together
64 determine the air quality in Beijing (Meng et al., 2006; Zhang et al., 2012).

65 Several studies have been performed to investigate the role of trans-boundary transport
66 in the air quality of Beijing based on observational analyses and model simulations. Using the
67 US EPA's Model-3/CMAQ model simulation in the Beijing area, Streets et al. (2007) have
68 pointed out that Hebei Province can contribute 50-70% of Beijing's $PM_{2.5}$ concentration and
69 20-30% of O_3 concentration. Wang et al. (2009) have indicated that O_3 formation in Beijing
70 is not only affected by local emissions, but also influenced by Tianjin and the south of Hebei
71 Province. The intense regional transport of pollutants from south to north in NCP has been
72 proposed to be the main reason for the heavy haze pollution in January 2013 in Beijing (Sun
73 et al., 2014; Tao et al., 2014; Wang et al., 2014b). Jiang et al. (2015) have demonstrated that
74 the transport from the environs of Beijing contributed about 55% of the peak $PM_{2.5}$
75 concentration in the city during a heavy haze event in December 2013.

Since September 2013, the 'Atmospheric Pollution Prevention and Control Action Plan' (hereafter referred to as APPCAP) has been implemented, which was released by the Chinese State Council to reduce $PM_{2.5}$ by up to 25% by 2017 relative to 2012 levels. After implementation of the APPCAP, high $PM_{2.5}$ mass concentrations still can be observed and the O_3 pollution has deteriorated during summertime since 2013 in Beijing (Chen et al., 2015; Wang et al., 2016). Hence, studies are imperative to explore the O_3 and $PM_{2.5}$ formation from various sources and evaluate the pollutants contributions from local production and trans-boundary transport in Beijing, to support the design of mitigation strategies.

The purpose of the present study is to evaluate the contributions of trans-boundary transport of emissions outside of Beijing to the air quality in Beijing and interaction of emissions in and outside of Beijing after APPCAP using the WRF-CHEM model. The model configuration and methodology are described in Section 2. Model results and sensitivity studies are presented in Section 3, and conclusions and discussions are given in Section 4.

2 Model and Methodology

2.1 WRF-CHEM Model

The WRF-CHEM model used in the study is developed by Li et al. (2010, 2011a, b, 2012) at the Molina Center for Energy and the Environment, with a new flexible gas phase chemical module and the CMAQ aerosol module developed by US EPA. The aerosol component of the Community Multiscale Air Quality (CMAQ) model is designed to be an efficient and economical depiction of aerosol dynamics in the atmosphere (Binkowski and Roselle, 2003). The particle size distribution in the study is represented as the superposition

of three lognormal subdistributions, called modes, which includes the processes of coagulation, particle growth by the addition of mass, and new particle formation. Following the work of Kulmala et al. (1998), the new particle production rate presented here is calculated as a parameterized function of temperature, relative humidity, and the vapor-phase H_2SO_4 concentration due to binary nucleation of H_2SO_4 and H_2O vapor, and the new particles are assumed to be 2.0 nm diameter. A number of recent studies have shown that organic compounds can play an important role in nucleation process (Zhang et al., 2009, 2012, 2015). The contribution from organic acids likely explains the high levels of aerosol, especially in polluted urban area, where large amount of organic acids can be emitted directly and produced by photochemical oxidation of hydrocarbons (Fan et al., 2006), which needs to be considered in the further study. The wet deposition follows the method used in the CMAQ and the surface deposition of chemical species is parameterized following Wesely (1989). The photolysis rates are calculated using the FTUV (Li et al., 2005; Li et al., 2011a), in which the effects of aerosols and clouds on photolysis are considered.

The inorganic aerosols are predicted in the WRF-CHEM model using ISORROPIA Version 1.7 (Nenes et al., 1998). The efficient and rapid secondary species formation in Beijing has been found during the severe haze formation process in the previous study (Guo et al., 2014). The secondary organic aerosol (SOA) formation is calculated using a non-traditional SOA module. The volatility basis-set (VBS) modeling method is used in the module, assuming that primary organic components are semi-volatile and photochemically reactive and are distributed in logarithmically spaced volatility bins. Detailed information about the volatility basis-set approach can be found in Li et al (2011b). Recent studies have

shown that small di-carbonyls (glyoxal and methylglyoxal) are important for the aerosol formation due to their traffic origin (Zhao et al., 2006; Gomez et al., 2015). Li et al. (2011a) have indicated that glyoxal and methylglyoxal can contribute about 10% of the SOA in the urban area of Mexico City. The SOA formation from glyoxal and methylglyoxal in this study is parameterized as a first-order irreversible uptake by aerosol particles and cloud droplets, with a reactive uptake coefficient of $3.7\times.7^{-3}$ for glyoxal and methylglyoxal (Zhao et al., 2006; Volkamer et al., 2007; Gomez et al., 2015).

2.2 Pollution Episode Simulation

A persistent air pollution episode from 5 to 14 July 2015 in Beijing-Tianjin-Hebei (BTH) is simulated using the WRF-CHEM model. During the episode, the observed mean daily $PM_{2.5}$ concentration is 73.8 μg m^{-3} and the average O_3 concentration in the afternoon reaches 237.0 μg m^{-3} in Beijing. The maximum of O_3 concentration is higher than 350 μg m^{-3}, and the maximum of $PM_{2.5}$ concentration can reach a high level exceeding 150 μg m^{-3}. SI-Figures 1a-c show the daily averages of the temperature, relative humidity, and wind speed in Beijing during the summer of 2015. The minimum air temperature is 18.7°C, and the maximum air temperature is 40 °C during the summer, with average of 25.7°C. The average relative humidity is 63.8%. The southeast or southwest wind is prevailing over NCP due to the influence of East Asian summer monsoon (Zhang et al., 2010), with the average wind speed of 5.6 m s^{-1} in the summer of 2015. During the study period, the average temperature, relative humidity, and wind speed are 28.4°C, 51.7% and 6.3 m s^{-1}, respectively, indicating typical summertime meteorological conditions. During the summer of 2015, the average $PM_{2.5}$ concentration is 56.1 μg m^{-3} and the average O_3 concentration in the afternoon is 216.4

142 μg m^{-3} (SI-Figures 1d-e). The high O_3 and $PM_{2.5}$ event occurs frequently during the
143 summertime of 2015, so the study period can well represent the summertime O_3 and $PM_{2.5}$
144 pollution in Beijing, and provide a suitable case for observation analyses and model
145 simulations to investigate the effect of trans-boundary transport on the summertime air
146 quality of Beijing.

147 The WRF-CHEM model adopts one grid with horizontal resolution of 6 km and 35
148 sigma levels in the vertical direction, and the grid cells used for the domain are 200 × 200
149 (Figure 1). The physical parameterizations include the microphysics scheme of Hong et al
150 (Hong and Lim, 2006), the Mellor, Yamada, and Janjic (MYJ) turbulent kinetic energy (TKE)
151 planetary boundary layer scheme (Janjić, 2002), the Unified Noah land-surface model (Chen
152 and Dudhia, 2001), the rapid radiative transfer model (RRTM) long wave radiation scheme
153 (Mlawer et al., 1997) and the Goddard shortwave parameterization (Suarex and Chou, 1994;
154 Chou and Suarez, 1999, 2001). The NCEP 1° × 1° reanalysis data are used to obtain the
155 meteorological initial and boundary conditions, and the meteorological simulations are not
156 nudged in the study. The chemical initial and boundary conditions are interpolated from the
157 6h output of MOZART (Horowitz et al., 2003). The spin-up time of the WRF-CHEM model
158 is 28 hours. The SAPRC-99 (Statewide Air Pollution Research Center, version 1999)
159 chemical mechanism is used in the present study.

160 The anthropogenic emissions are developed by Zhang et al. (2009), which is based on
161 the 2013 emission inventory, including contributions from agriculture, industry, power
162 generation, residential, and transportation sources. The SO_2, NO_x, and CO emissions have
163 been adjusted according to their observed trends from 2013 to 2015 in the present study, but

the VOCs emissions are not changed considering that the VOCs emissions are still not fully considered in the current air pollutant control strategy. The major pollutants emissions used in the model simulation for Beijing, Tianjin, and the neighboring provinces (Hebei, Shanxi, and Shandong) are summarized in Table 1. Obviously, high anthropogenic emissions are distributed outside of Beijing, especially in Hebei and Shandong provinces. Figure 2 presents distributions of the emission rates of VOCs, NO_x, OC, and SO_2 in the simulation domain, showing that the anthropogenic emissions are generally concentrated in urban areas. As shown in Figure 2, the total emissions from neighboring regions are much more than those in Beijing, and the emission rates in Tianjin, the south of Hebei and Shandong are also higher than those in Beijing, particularly with regard to SO_2 emissions. Therefore, when the south or east wind is prevailing in NCP, the severe air pollution can be formed in Beijing when precursor emissions in highly industrialized areas chemically react as they are carried toward Beijing, blocked by mountains and further accumulated and interacted with those in Beijing. It is worth noting that uncertainties of the emission inventory used in the study are still rather large taking consideration of the rapid changes in anthropogenic emissions that are not fully reflected in the current emission inventories, particularly since implementation of the APPCAP, and the complexity of pollutants precursors. For example, different VOCs types exhibit distinct kinetic behaviors, and as an important fraction of total VOCs in the urban atmosphere, aromatics are responsible for the photochemical ozone production and secondary organic aerosol formation (Suh et al., 2003; Fan et al., 2004). In the SAPRC99, aromatics are lumped into ARO1 and ARO2. ARO1 mainly includes toluene, benzene, ethylbenzene, and other aromatics with reaction rate with OH (kOH) less than 2×10^4 ppm^{-1} min^{-1}. ARO2

includes xylene, trimethylbenzene, and other aromatics with kOH greater than 2×10^4 ppm^{-1} min^{-1}. Additionally, biogenic VOCs also play a considerable role in the ozone production (Li et al., 2007), and monoterpenes and isoprene are the main biogenic VOCs in the SAPRC99 chemical mechanism. The biogenic emissions are calculated online using the MEGAN (Model of Emissions of Gases and Aerosol from Nature) model developed by Guenther et al (2006).

2.3 Factor Separation Approach

The formation of the secondary atmospheric pollutant, such as O_3, secondary organic aerosol, and nitrate, is a complicated nonlinear process in which its precursors from various emission sources and transport react chemically or reach equilibrium thermodynamically. Nevertheless, it is not straightforward to evaluate the contributions from different factors in a nonlinear process. The factor separation approach (FSA) proposed by Stein and Alpert (1993) can be used to isolate the effect of one single factor from a nonlinear process and has been widely used to evaluate source effects (Gabusi et al., 2008; Weinroth et al., 2008; Carnevale et al., 2010; Li et al., 2014). The total effect of one factor in the presence of others can be decomposed into contributions from the factor and that from the interactions of all those factors.

Suppose that field $\boldsymbol{f}$ depends on a factor $\boldsymbol{\varphi}$:

$$\boldsymbol{f} = \boldsymbol{f}(\boldsymbol{\varphi})$$

The FSA decomposes function $\boldsymbol{f}(\boldsymbol{\varphi})$ into a constant part that does not depend on $\boldsymbol{\varphi}$ $(\boldsymbol{f}(\mathbf{0}))$ and a $\boldsymbol{\varphi}$-depending component $(\boldsymbol{f}'(\boldsymbol{\varphi}))$, as follows:

$$\boldsymbol{f}'(\mathbf{0}) = \boldsymbol{f}(\mathbf{0})$$

$$\boldsymbol{f'(\varphi) = f(\varphi) - f(0)}$$

Considering that there are two factors *X* and *Y* that influence the formation of secondary pollutants in the atmosphere and also interact with each other. Denoting $\boldsymbol{f_{XY}}$, $\boldsymbol{f_X}$, $\boldsymbol{f_Y}$, and $\boldsymbol{f_0}$ as the simulations including both of two factors, factor *X* only, factor *Y* only, and none of the two factors, respectively. The contributions of factor *X* and *Y* can be isolated as follows:

$$\boldsymbol{f'_X = f_X - f_0}$$

$$\boldsymbol{f'_Y = f_Y - f_0}$$

Note that term $\boldsymbol{f'_{X(Y)}}$ represents the impacts of factor *X(Y)*, while $\boldsymbol{f_0}$ is the term independent of factors *X* and *Y*.

The simulation including both factors *X* and *Y* is given by:

$$\boldsymbol{f_{XY} = f_0 + f'_X + f'_Y + f'_{XY}}$$

The mutual interaction between *X* and *Y* can be expressed as:

$$\boldsymbol{f'_{XY} = f_{XY} - f_0 - f'_X - f'_Y = f_{XY} - (f_X - f_0) - (f_Y - f_0) - f_0 = f_{XY} - f_X - f_Y + f_0}$$

The above equation shows that the study needs four simulations, $\boldsymbol{f_{XY}}, \boldsymbol{f_X}, \boldsymbol{f_Y}$ and $\boldsymbol{f_0}$, to evaluate the contributions of two factors and their synergistic interactions.

2.4 Statistical Metrics for Observation-Model Comparisons

In the present study, the mean bias (*MB*), root mean square error (*RMSE*) and the index of agreement (*IOA*) are used as indicators to evaluate the performance of WRF-CEHM model in simulation against measurements. *IOA* describes the relative difference between the model and observation, ranging from 0 to 1, with 1 indicating perfect agreement.

$$MB = \frac{1}{N}\sum_{i=1}^{N}(P_i - O_i)$$

$$RMSE = \left[\frac{1}{N}\sum_{i=1}^{N}(P_i - O_i)^2\right]^{\frac{1}{2}}$$

$$IOA = 1 - \frac{\sum_{i=1}^{N}(P_i - O_i)^2}{\sum_{i=1}^{N}(|P_i - \bar{O}| + |O_i - \bar{O}|)^2}$$

where P_i and O_i are the predicted and observed pollutant concentrations, respectively. *N* is the total number of the predictions used for comparisons, and $\bar{P}$ and $\bar{O}$ represents the average of the prediction and observation, respectively.

2.5 Pollutant Measurements

The hourly measurements of O_3, NO_2, and $PM_{2.5}$ used in the study are downloaded from the website http://www.aqistudy.cn/. The submicron sulfate, nitrate, ammonium, and organic aerosols are observed by the Aerodyne Aerosol Chemical Speciation Monitor (ACSM), which is deployed at the National Center for Nanoscience and Technology (NCNST), Chinese Academy of Sciences, Beijing (Figure 1). The mass spectra of organic aerosols are analyzed using the Positive Matrix Factorization (PMF) technique to separate into four components: hydrocarbon-like organic aerosol (HOA)，cooking organic aerosol (COA)，coal combustion organic aerosol (CCOA), and oxygenated organic aerosol (OOA). HOA, COA, and CCOA are interpreted as surrogates of primary organic aerosol (POA), and OOA is a surrogate of SOA.

The APPCAP has been implemented since 2013 September, so comparisons of summertime pollutants between 2013 and 2015 can show the mitigation effects on the air quality. Considering that high O_3 concentrations generally take place in the afternoon during summertime, Table 2 presents the summertime concentrations of pollutants in the afternoon (12:00 – 18:00 Beijing Time (BJT)) averaged at 12 monitoring sites in Beijing in 2013 and 2015. The rainy days during summertime in Beijing are 43 and 46 days in 2013 and 2015, respectively, showing the similar meteorological conditions between the two years. Therefore,

252 in general, the air pollutants variations between 2013 and 2015 can be mainly attributed to
253 implementation of the APPCAP. Apparently, implementation of the APPCAP has
254 considerably decrease the concentrations of primary species of CO and SO_2, particularly with
255 regard to SO_2, reduced by more than 40% from 2013 to 2015. Most of NO_x exist in the form
256 of NO_2 in the afternoon during summertime due to active photochemical processes. Therefore,
257 25.1% decrease of NO_2 in the afternoon from 2013 to 2015 shows that the NO_x emission
258 mitigation is also effective in Beijing. The $PM_{2.5}$ concentrations are decreased by about 24.0%
259 from 2013 to 2015, approaching the expected 25% reduction by 2017 relative to 2012 levels.
260 However, the O_3 trend is not anticipated in Beijing, and O_3 concentrations are increased from
261 133.0 μg m^{-3} in 2013 to 163.2 μg m^{-3} in 2015, enhanced by 22.8%. For the discussion
262 convenience, we have defined the O_3 exceedance with hourly O_3 concentrations exceeding
263 200 μg m^{-3} and $PM_{2.5}$ exceedance with hourly $PM_{2.5}$ concentrations exceeding 75 μg m^{-3}.
264 Although the $PM_{2.5}$ exceedance frequency in the afternoon has been decreased by 25.0%
265 from 2013 to 2015, but still remains 32.7% in 2015. The O_3 exceedance frequency in 2015 is
266 31.8%, enhanced by 57.6% compared to 20.2% in 2013. Hence, during the summertime of
267 2015, two years after implementation of the APPCAP, Beijing still has experienced high O_3
268 and/or $PM_{2.5}$ pollutions frequently.
269

270 **3 Results and Discussions**

271 **3.1 Model Performance**

272 The hourly measurements of O_3, NO_2, and $PM_{2.5}$ in Beijing-Tianjin-Hebei (BTH) and
273 ACSM measured aerosol species in Beijing are used to validate the WRF-CHEM model

274 simulations.

275 **3.1.1 O_3, NO_2, and $PM_{2.5}$ Simulations in Beijing**

276 Figure 3 shows the temporal variations of observed and simulated near-surface O_3, NO_2,
277 and $PM_{2.5}$ concentrations averaged over monitoring sites in Beijing from 5 to 14 July 2015.
278 The WRF-CHEM model performs reasonably well in simulating the $PM_{2.5}$ variations
279 compared with observations in Beijing. The *MB* and *RMSE* are -3.6 μg m^{-3} and 22.5 μg m^{-3},
280 respectively, and the *IOA* is 0.86. The model well reproduces the temporal variations of O_3
281 concentrations, with an *IOA* of 0.92. The model considerably underestimates the O_3
282 concentration during daytime on July 5, 6 and 13. Most of monitoring sites in Beijing are
283 concentrated in the urban area. Therefore, if the simulated winds cause the O_3 plume formed
284 in the urban area to leave early or deviate the O_3 plume transported from outside of Beijing
285 from the urban area, the model is subject to underestimate the O_3 concentration in Beijing
286 (Bei et al., 2010). The WRF-CHEM model also reasonably yields the NO_2 diurnal profiles,
287 but frequently overestimates the NO_2 concentrations during nighttime, which is likely caused
288 by the biased boundary layer simulations.

289 **3.1.2 Aerosol Species Simulations in Beijing**

290 Figure 4 shows the temporal variations of simulated and observed aerosol species at
291 NCNST site in Beijing from 5 to 14 July 2015. The WRF-CHEM model generally performs
292 reasonably in simulating the aerosol species variations compared with ACSM measurements.
293 As a primary aerosol species, the POA in Beijing is determined by direct emissions from
294 various sources and transport from outside of Beijing, so uncertainties from emissions and
295 meteorological fields remarkably affect the model simulations (Bei et al., 2012, 2013).

296 Although the *MB* and *RMSE* for POA are 0.0 μg m^{-3} and 3.1 μg m^{-3}, respectively, the *IOA* is
297 less than 0.60, indicating the considerable biases in POA simulations. The WRF-CHEM
298 model has difficulties in well simulating the sulfate aerosol, with an *IOA* lower than 0.60.
299 The model cannot produce the observed high peaks of sulfate aerosols around noontime on 8,
300 11, and 12 July 2015. The sulfate aerosol in the atmosphere is produced from multiple
301 sources, including SO_2 gas-phase oxidations by hydroxyl radicals (OH) and stabilized criegee
302 intermediates (sCI), aqueous reactions in cloud or fog droplets, and heterogeneous reactions
303 on aerosol surfaces, as well as direct emissions from power plants and industries (Li et al.,
304 2016). The model reasonably well reproduces the observed temporal variations of SOA,
305 nitrate, and ammonium, with *IOA*s exceeding 0.75. The model simulate well the peak
306 concentration of SOA, nitrate and ammonium at the rush hour, but the model also
307 underestimates the SOA, nitrate and ammonium as well, with *MB* of -1.1 μg m^{-3}, -0.7 μg m^{-3},
308 and -0.5 μg m^{-3}, respectively. For nitrate and ammonium, the underestimates occur mainly on
309 8 July 2015 possibly due to wind filed, which will be further analyzed in supplement
310 (SI-Figure 2).

311 **3.1.3 O_3, NO_2, and $PM_{2.5}$ Simulations in BTH**

312 Figure 5 shows the diurnal profiles of observed and simulated near-surface O_3, NO_2,
313 and $PM_{2.5}$ concentrations averaged over monitoring sites in BTH from 5 to 14 July 2015. The
314 WRF-CHEM model exhibits good performance in predicting the temporal variations of O_3,
315 NO_2, and $PM_{2.5}$ concentrations compared with measurements in BTH, with *IOA*s higher than
316 0.80. In addition, O_3 and NO_2 simulations are also improved in BTH compared to those in
317 Beijing, indicating better model performance for regional simulations in a large scale.

Figure 6 presents the distributions of calculated and observed near-surface $PM_{2.5}$ concentrations along with the simulated wind fields at 10:00 Beijing Time (BJT) on the six selected representative days with high O_3 and $PM_{2.5}$ concentrations. The calculated $PM_{2.5}$ spatial patterns generally agree well with the observations at the monitoring sites. The observed $PM_{2.5}$ concentrations in BTH are still high even after implementation of the APPCAP, frequently exceeding 75 μg m^{-3} on the selected six days. The $PM_{2.5}$ concentrations in Beijing are higher than 115 μg m^{-3} at 10:00 BJT on 8, 11, and 12 July 2015, causing moderate air pollution.

The O_3 concentration during summertime reaches its peak during the period from 14:00 to 16:00 BJT in Beijing (Tang et al., 2012). Figure 7 presents the spatial distribution of calculated and measured near-surface O_3 concentration at 15:00 Beijing Time (BJT) on the selected six days, along with the simulated wind fields. In general, the simulated O_3 spatial patterns are consistent with the measurements, but model biases still exist. High O_3 concentrations at 15:00 BJT in Beijing are observed and also simulated by the model, frequently exceeding 250 μg m^{-3}. The O_3 transport to Beijing from its surrounding areas is also obvious when the winds are easterly or southerly. Figure 8 provides the spatial distribution of simulated and observed near-surface NO_2 concentration on the selected six days at 08:00 BJT when the NO_2 concentration reaches it peak due to rush hour NO_x emissions and low planetary boundary layer (PBL). The simulated near-surface NO_2 concentrations highlights the dominant impact of the anthropogenic emissions, primarily concentrated in cities or their downwind areas, which generally agree well with the measurements. Beijing is surrounded from south to east by cities with high NO_2

concentrations, which can influence the O_3 formation in Beijing when south or east winds are prevalent.

The good agreements between predicted $PM_{2.5}$, O_3, NO_x and aerosol species and the corresponding measurements show that the modeled meteorological fields and emissions used in simulations are generally reasonable.

3.2 Contributions of Trans-boundary Transport to the O_3 and $PM_{2.5}$ Levels in Beijing

3.2.1 Analysis of Horizontal Transport of O_3 and $PM_{2.5}$

The analysis in Section 3.1.3 has shown the strong correlation between the airflow and the high level of pollutants in Beijing during the study episode. It is essential to confirm whether the continuous air pollutions in Beijing are directly related to the airflow transport from outside of Beijing (An et al., 2007; Yang et al., 2010). In the present study, the horizontal transport flux intensity is defined as the horizontal wind speed on the grid border multiplied by the pollutants concentration of the corresponding grid from which the airflows comes (Jiang et al., 2008). Considering that trans-boundary transport mainly occurs within the PBL, the study also focuses on the contribution of trans-boundary transport of pollutants within PBL over Beijing and its surrounding areas. Previous studies have shown that the average mixing layer height is approximately between 600—800 m during summertime, with the maximum during noontime higher than 1000 m (Wang et al.,2015; Tang et al., 2016). Figure 9 shows the temporal variations of net horizontal transport flux of $PM_{2.5}$, O_3 and NO_2 through Beijing boundary and the pollutants contributions from non-Beijing emissions to the air quality in Beijing city. The hourly $PM_{2.5}$, O_3 and NO_2 contributions of non-Beijing emissions generally have the same variation trend as the horizontal transport flux, indicating

that the contribution of surrounding sources plays an important role in high pollutants concentrations in Beijing during the study episode. For example, the O_3 net flux also has the similar peak in the afternoon as the O_3 contribution from the non-Beijing emissions. As discussed in Section 3.1.3, the prevailing south wind dominates in BTH, so the largest flux intensity are from the south, with the average of 103.3 g s^{-1} and 244.5 g s^{-1} for $PM_{2.5}$ and O_3, respectively (SI-Table 1), indicating that the pollutants are mainly from the south. It should be noted that the flux of O_3 is mainly focused on the afternoon from 12:00 to 18:00 BJT. The average net horizontal transport fluxes for $PM_{2.5}$ and O_3 during the episode are 68.2 g s^{-1} and 68.5 g s^{-1}, respectively, showing important contributions of non-Beijing emissions to the air quality in Beijing.

3.2.2 Trans-boundary Transport Contributions to O_3 in Beijing

The FSA is used in the present study to evaluate the contributions and interactions of emissions from Beijing and outside of Beijing to the near-surface concentrations of O_3 and $PM_{2.5}$ in Beijing. Four model simulations are performed, including $\boldsymbol{f_{BS}}$ with both the anthropogenic emissions from Beijing and outside of Beijing, $\boldsymbol{f_B}$ with the emission from Beijing alone, $\boldsymbol{f_S}$ with only emissions outside of Beijing, and $\boldsymbol{f_0}$ without both the emissions from Beijing and outside of Beijing, representing background concentrations. Apparently, the air pollutants levels in Beijing are determined by the contribution from local emissions ($\boldsymbol{f'_B}$, $\boldsymbol{f_B - f_0}$), the trans-boundary transport of non-Beijing emissions ($\boldsymbol{f'_S}$, $\boldsymbol{f_S - f_0}$), emission interactions between local and non-Beijing emissions ($\boldsymbol{f'_{BS}}$, $\boldsymbol{f_{BS} - f_B - f_S + f_0}$), and background ($\boldsymbol{f_0}$).

Figure 10 provides the temporal variations of the average near-surface O_3 and $PM_{2.5}$

concentrations from f_{BS} with all the emissions, f_B with Beijing emissions alone, and f_S with non-Beijing emissions alone in Beijing from 5 to 14 July 2015. Apparently, non-Beijing emissions generally play a more important role in the O_3 level of Beijing than local emissions. Even when the Beijing local emissions are excluded, the O_3 concentration in Beijing still remains high level, with an average of 153 μg m^{-3} and ranging from 130 to 180 μg m^{-3} in the afternoon. When only considering the Beijing local emission in simulations, the afternoon average O_3 concentration in Beijing is approximately 126.6 μg m^{-3}, varying from 80 to 160 μg m^{-3}. On July 13, the contribution from Beijing local emissions exceeds that from non-Beijing emissions because north winds are prevailing, bringing clean air to Beijing (Figure 7f). Table 3 gives the average O_3 contributions from 12:00 to 18:00 BJT in Beijing from local emissions, non-Beijing emissions, emission interactions, and background. The local emissions contribute about 22.4% on average in the afternoon to the O_3 level in Beijing, varying from 15.5% to 35.4%. The non-Beijing emissions contribute more than local sources, with an average contribution of 36.6%, ranging from 15.2% to 48.0%. The emission interactions in Beijing decrease the O_3 level by 5.1% on average. O_3 formation is a nonlinear process, depending on not only the absolute levels of NO_x and VOCs, but also the ratio of VOC_s/NO_x (Sillman et al., 1990; Lei et al., 2007, 2008). When the O_3 precursors emitted from outside of Beijing are transported to Beijing and mixed with local emissions, the concentrations of O_3 precursors are increased and the ratio of VOC_s/NO_x is also altered, causing the formed O_3 concentration unequal to the simple linear summation of O_3 contributions from the local and non-Beijing emissions. The background O_3 in Beijing plays an important role in the O_3 level in the afternoon, accounting for 46.1% of the O_3

concentration. The background O_3 contribution varies from 32.6% to 62.9% during the episode, which is primarily determined by the prevailing wind direction. When the northerly wind is prevalent, the clean airflow from the north affects Beijing, enhancing the background O_3 contribution, such as on 5, 13, and 14 July 2015. However, when the polluted airflow from the south impacts Beijing, the background O_3 contribution is decreased. The O_3 contributions in Beijing induced by the trans-boundary transport of emissions outside of Beijing is about 31.5% of the O_3 concentration during the study episodes, which is in agreement with previous studies (Streets et al., 2007; Wang et al., 2008), indicating that the trans-boundary transport constitutes the main reason for the elevated O_3 level in Beijing after implementation of the APPCAP.

Previous studies have proposed that the regional transport of O_3 precursors can play an important role in inducing the high O_3 concentrations level in Beijing (Wang et al., 2009; Zhang et al., 2014). SI-Table 2 provides the average NO_2 contributions in Beijing from local emissions, non-Beijing emissions, emission interactions, and background. Different from O_3, the local emissions dominate the level of NO_2 in Beijing area, with an average contribution of 70.3% during the study episode. The average contribution of non-Beijing emissions, emission interactions and background are 24.8%, 0.9% and 4.0%, respectively.

3.2.3 Trans-boundary Transport Contributions to $PM_{2.5}$ in Beijing

When the Beijing local emissions are not considered in simulations, Beijing still experiences high $PM_{2.5}$ pollution, with an average $PM_{2.5}$ concentration of 48.3 μg m^{-3} during the simulation episode, and the $PM_{2.5}$ level in Beijing still exceeds 75 μg m^{-3} on several days. However, when only considering the Beijing local emissions, the average $PM_{2.5}$

concentration in Beijing is 19.6 μg m^{-3} during the episode, showing that Beijing's $PM_{2.5}$ pollution is dominated by the trans-boundary transport (Figure 10b). Table 4 shows the average $PM_{2.5}$ contribution in Beijing from local emissions, non-Beijing emissions, emission interactions, and background. During the study episode, the average $PM_{2.5}$ contribution from local emissions is 13.7%, which is much lower than the contribution of 61.5% from non-Beijing emissions, further showing the dominant role of the trans-boundary transport in the Beijing $PM_{2.5}$ pollution. The emission interactions enhance the $PM_{2.5}$ level in Beijing on average, with a contribution of 5.9%. The background $PM_{2.5}$ contribution to Beijing is 18.9% on average, lower than those for O_3. The $PM_{2.5}$ contribution caused by the trans-boundary transport is about 67.4% of $PM_{2.5}$ concentrations in Beijing, indicating that the cooperation with neighboring provinces to control the $PM_{2.5}$ level is a key for Beijing to improve air quality. Previous studies have also demonstrated the dominant role of non-Beijing emissions in the $PM_{2.5}$ level in Beijing. Based on CMAQ model, Streets et al. (2007) have reported that average contribution of regional transport to $PM_{2.5}$ at the Olympic Stadium can be 34%, up to 50%—70% under prevailing south winds. Guo et al. (2010) have provided a rough estimation that the regional transport can contribute 69% of the PM_{10} and 87% of the $PM_{1.8}$ in Beijing local area using the short and low time resolution data in the summer. Combining the $PM_{2.5}$ observations and MM5-CMAQ model results, regional transport is estimated to contribute 54.6% of the $PM_{2.5}$ concentration during the polluted period, with an annual average $PM_{2.5}$ contribution of 42.4% (Lang et al., 2013). Using the long-term measurements of $PM_{2.5}$ mass concentrations from 2005 to 2010 at urban Beijing, and trajectory cluster and receptor models, the average contribution of long-distance transport to Beijing's $PM_{2.5}$ level can be

approximately 75.2% in the summer (Wang et al., 2015).

3.2.4 Trans-boundary Transport Contributions to Aerosol Species in Beijing

Figure 11 shows the temporal variation of the averaged contributions to the near-surface aerosol constituents from total emissions ($\boldsymbol{f_{BS}}$), local emissions ($\boldsymbol{f'_B}$), the trans-boundary transport of non-Beijing emissions ($\boldsymbol{f'_S}$), emission interactions ($\boldsymbol{f'_{BS}}$), and the background ($\boldsymbol{f_0}$) during the simulation episode. The temporal variations of elemental carbon (EC) and POA from local emissions and trans-boundary transport exhibit obvious diurnal cycles, i.e., highest during nighttime and lowest in the afternoon, corresponding to the variations of PBL height and anthropogenic emissions. The SOA from local emissions reaches its peak in the afternoon when the O_3 concentration is high, but the trans-boundary transport causes the gradual accumulation process of SOA in Beijing from July 5 to 9 and from July 9 to 13. The sulfate temporal profile from the trans-boundary transport is similar to that of SOA, also showing the accumulation process. In addition, the sulfate aerosols from local emissions do not vary remarkably. The nitrate aerosols from local emissions and the trans-boundary transport generally attain peaks in the morning when the air temperature is not high and the HNO_3 concentrations are not low. The ammonium aerosol variations are generally determined by those of sulfate and nitrate aerosols. For example, the variations of ammonium aerosols from the trans-boundary include not only the morning peaks, but also the accumulation processes from July 5 to 9 and from July 9 to 13. Except the sulfate aerosol, the temporal variations of aerosol species from background are not large.

Table 5 presents the average aerosol constituents contributions from Beijing local emissions, non-Beijing emissions, emission interactions, and the background, and mass

fractions in the total $PM_{2.5}$ in Beijing during the episode. Organic aerosols (POA+SOA) constitute the most important component of $PM_{2.5}$, accounting for 34.8% of $PM_{2.5}$ mass concentration, which is consistent with the ACSM measurement in Beijing (Sun et al., 2014). In addition, SOA contributes more than 70% of organic aerosol mass concentrations. Although the SO_2 concentrations have been decreased by more than 40% since implementation of the APPCAP, sulfate aerosols still play an important role in the $PM_{2.5}$ level in Beijing and make up 25.1% of the $PM_{2.5}$ mass concentrations, showing high sulfate contributions from the trans-boundary transport and background. The ammonium, nitrate, EC, and unspecified species account for 13.7%, 14.1%, 5.8%, and 6.5% of the $PM_{2.5}$ mass concentrations, respectively. Secondary aerosol species dominate the $PM_{2.5}$ mass concentration in Beijing, with a contribution of 77.9%.

The local emissions contribute more than 20% of the mass concentrations for the primary aerosol species, but less than 15% for the secondary aerosol species in Beijing (Table 5). The trans-boundary transport of non-Beijing emissions dominates all the aerosol species levels in Beijing, with contributions exceeding 50%, particularly for SOA and nitrate. In addition, the POA and sulfate background contributions are also high, more than 20%. Although the primary aerosol species of EC and unspecified constituents are not involved in the chemical process and also do not participate in the gas-particle partitioning, the emission interactions still enhance EC and unspecified constituents concentrations, with contributions of around 1.5%, which is caused by the PBL-pollution interaction. It is clear that the PBL-pollution interaction plays an important role in the pollutant accumulation in Beijing (Wang et al., 2013; Peng et al., 2016). Mixing of Beijing local emissions with those outside

494 of Beijing increases the aerosol concentrations in the PBL and decreases the incoming solar
495 radiation down to the surface, cooling the temperature of the low level atmosphere to
496 suppress the development of PBL and hinder the aerosol dispersion in the vertical direction.

497 The emission interactions increase the POA and SOA concentrations, with a POA
498 contribution of 5.3% and a SOA contribution of 5.9%. In the VBS modeling approach,
499 primary organic components are assumed to be semi-volatile and photochemically reactive.
500 Mixing of Beijing local emissions with non-Beijing emissions enhances the organic
501 condensable gases, and considering that the saturation concentrations of the organic
502 condensable gases do not change, more organic condensable gases partition into the particle
503 phase, increasing the POA and SOA concentrations.

504 The contributions of emission interactions to inorganic aerosols, including sulfate,
505 nitrate, and ammonium are more complicated, depending on their particle phase and
506 precursors concentrations. In the present study, ISORROPIA (Version 1.7) is used to
507 calculate the thermodynamic equilibrium between the sulfate-nitrate-ammonium-water
508 aerosols and their gas phase precursors H_2SO_4-HNO_3-NH_3-water vapor. Although mixing of
509 Beijing local emissions with non-Beijing emissions increases inorganic aerosols precursors,
510 the inorganic aerosol contributions from emission interactions are still uncertain due to the
511 thermodynamic equilibrium between inorganic aerosols and their precursors. The nitrate
512 contributions from emission interactions are 18.1%, much more than those for other aerosol
513 constituent. The sulfate contribution from emission interactions is not significant, only 3.4%.
514 The ammonium contributions from emissions interactions are 1.5%, similar to those of
515 primary aerosol species.

4 Summary and Conclusions

In the present study, a persistent air pollution episode with high concentrations of O_3 and $PM_{2.5}$ is simulated using the WRF-CHEM model during the period from July 5 to 14, 2015 in BTH, to evaluate the contributions of trans-boundary transport to the air quality in Beijing. Although the APPCAP has been implemented since 2013 September, the average O_3 concentration in the afternoon has increased by 22.8% from 2013 to 2015 in Beijing, and Beijing still has experienced high O_3 and/or $PM_{2.5}$ concentrations frequently during summertime of 2015.

In general, the predicted temporal variations of $PM_{2.5}$, O_3, and NO_2 concentrations agree well with observations in Beijing and BTH, but the model biases still exist, which is perhaps caused by the uncertainties of simulated meteorological conditions and the emission inventory. The model also successfully reproduces the spatial distributions of $PM_{2.5}$, O_3, and NO_2 concentrations compared with measurements. The model performs reasonably well in modeling the variations of aerosol constituents compared with ACSM measurement at NCNST site in Beijing, but there are considerable biases in POA and sulfate simulations.

The FSA is used to investigate the contribution of trans-boundary transport of non-Beijing emissions to the air quality in Beijing. If the Beijing local emissions are not included in model simulations, the O_3 and $PM_{2.5}$ concentrations in Beijing still remain high, showing that the trans-boundary transport of emissions outside of Beijing plays a more important role in the air quality in Beijing than the Beijing local emissions. On average, the local emissions contribute 22.4% of O_3 in the afternoon and 13.7% of $PM_{2.5}$ mass concentrations in Beijing during the episode. The O_3 contribution in the afternoon and $PM_{2.5}$

contribution from the trans-boundary transport of non-Beijing emissions are 36.6% and 61.5%, respectively, far exceeding those from local emissions. The interactions between local and non-Beijing emissions generally decrease the O_3 level in the afternoon and increase the $PM_{2.5}$ level in Beijing during the episode, with contributions of -5.1% and +4.4%, respectively. In addition, the trans-boundary transport dominates all the aerosol species levels in Beijing, with contributions exceeding 50% on average, particularly for SOA and nitrate. The emission interactions in general increase all the aerosol species levels due to the PBL-pollution interaction and the enhancement of precursors of secondary aerosols. Hence, the air quality in Beijing during summertime is generally determined by the trans-boundary transport of emissions outside of Beijing.

However, it is still controversial on whether local or non-local emissions play a dominant role in the air quality in Beijing (Guo et al., 2010, 2014; Li et al., 2015; Zhang et al., 2015). When only considering the local emissions, the summertime $PM_{2.5}$ level in Beijing is comparable to that in Mexico City. Mexico City has once been one of the most polluted cities in the world, but the air quality has been greatly improved in recent years after taking emission control strategies (Molina et al., 2002, 2007, 2010). Therefore, a comprehensive model comparison of summertime pollution in Mexico City and Beijing would be illuminating for elucidation of the contributions of trans-boundary transport to the air quality in Beijing.

It is worth noting that, although the WRF-CHEM model well captures the spatial distributions and temporal variations of pollutants, the model biases still exist. The discrepancies between the predictions and observations are possibly caused by the

uncertainties in the emission inventory and the meteorological fields simulations (Zhang et al., 2015). BTH has been considered as a polluted air basin (Zhao et al., 2009; Parrish et al., 2015), which frequently experience O_3 and $PM_{2.5}$ pollutions during summertime. Future studies need to be conducted to improve the WRF-CHEM model simulations, and further to assess the contributions of trans-boundary transport of emissions outside of Beijing to the air quality in Beijing, considering the rapid changes in anthropogenic emissions since implementation of the APPCAP. This study mainly aims at providing a quantification of the effect of trans-boundary transport on the air quality in Beijing. It demonstrates that the effective approach to improve air quality in Beijing is to reduce both local and non-Beijing emissions in BTH. Further sensitivity simulations of different emission reduction measures are needed to design the most efficient emission control strategies.

572

573

574 Data availability: The real-time O_3 and $PM_{2.5}$ are accessible for the public on the website
575 http://106.37.208.233:20035/. One can also access the historic profile of observed ambient
576 pollutants through visiting http://www.aqistudy.cn/.

577

578 *Acknowledgements.* This work was supported by the National Natural Science Foundation of
579 China (No. 41275153) and supported by the "Strategic Priority Research Program" of the
580 Chinese Academy of Sciences，Grant No. XDB05060500. Guohui Li is also supported by the
581 “Hundred Talents Program” of the Chinese Academy of Sciences. Naifang Bei is supported
582 by the National Natural Science Foundation of China (No. 41275101).

583

584 **Reference**

585 An, X., Zhu, T., Wang, Z., Li, C., and Wang, Y.: A modeling analysis of a heavy air
586 pollution episode occurred in Beijing, Atmospheric Chemistry and Physics, 7, 3103-3114,
587 2007.

588 Bei, N., Lei, W., Zavala, M., and Molina, L. T.: Ozone predictabilities due to meteorological
589 uncertainties in the Mexico City basin using ensemble forecasts, Atmospheric Chemistry
590 and Physics, 10, 6295-6309, 10.5194/acp-10-6295-2010, 2010.

591 Bei, N., Li, G., and Molina, L. T.: Uncertainties in SOA simulations due to meteorological
592 uncertainties in Mexico City during MILAGRO-2006 field campaign, Atmospheric
593 Chemistry and Physics, 12, 11295-11308, 10.5194/acp-12-11295-2012, 2012.

594 Bei, N. F., Li, G. H., Zavala, M., Barrera, H., Torres, R., Grutter, M., Gutierrez, W., Garcia,
595 M., Ruiz-Suarez, L. G., Ortinez, A., Guitierrez, Y., Alvarado, C., Flores, I., and Molina, L.
596 T.: Meteorological overview and plume transport patterns during Cal-Mex 2010,
597 Atmospheric Environment, 70, 477-489, 10.1016/j.atmosenv.2012.01.065, 2013.

598 Binkowski, F. S. and Roselle S. J.: Models-3 Community Multiscale Air Quality (CMAQ)
599 model aerosol component: 1. Model description, Journal of Geophysical Reseasrch
600 Atmospheres, 108, 4183, doi:10.1029/2001JD001409, 2003.

601 Carnevale, C., Pisoni, E., and Volta, M.: A non-linear analysis to detect the origin of PM_{10}
602 concentrations in Northern Italy, Science of Total Environment, 409, 182-191,
603 http://dx.doi.org/10.1016/j.scitotenv.2010.09.038, 2010.

604 Chen, F., and Dudhia, J.: Coupling an advanced land surface-hydrology model with the Penn
605 State-NCAR MM5 modeling system. Part I: Model implementation and sensitivity,
606 Monthly Weather Review, 129, 569-585,
607 10.1175/1520-0493(2001)129<0569:caalsh>2.0.co;2, 2001.

608 Chen, W., Yan, L., and Zhao, H. M.: Seasonal Variations of Atmospheric Pollution and Air
609 Quality in Beijing, Atmosphere, 6, 1753-1770, 10.3390/atmos6111753, 2015.

610 Chou, M. D., and Suarez, M. J.: A solar radiation parameterization for atmospheric studies,
611 NASA TM-104606, Nasa Tech.memo, 15, 1999.

612 Chou, M. D., Suarez, M. J., Liang, X. Z., Yan, M. H., and Cote, C.: A Thermal Infrared
613 Radiation Parameterization for Atmospheric Studies, Max J, 2001.

614 Fan, J. W., and Zhang, R. Y.: Atmospheric Oxidation Mechanism of Isoprene, Environmental.
615 Chemistry, 1, 140-149, 10.1071/en04045, 2004.

616 Fan, J. W., Zhang, R. Y., Collins, D., and Li, G. H.: Contribution of secondary condensable
617 organics to new particle formation: A case study in Houston, Texas, Geophysical
618 Research Letters, 33, 4, 10.1029/2006gl026295, 2006.

619 Gabusi, V., Pisoni, E., and Volta, M.: Factor separation in air quality simulations, Ecological
620 Modelling, 218, 383-392, http://dx.doi.org/10.1016/j.ecolmodel.2008.07.030, 2008.

621 Gomez, M. E., Lin, Y., Guo, S., and Zhang, R. Y.: Heterogeneous Chemistry of Glyoxal on
622 Acidic Solutions. An Oligomerization Pathway for Secondary Organic Aerosol

623 Formation, Journal of Physical Chemistry. A, 119, 4457-4463, 10.1021/jp509916r, 2015.

624 Guenther, A., Karl, T., Harley, P., Wiedinmyer, C., Palmer, P. I., and Geron, C.: Estimates of
625 global terrestrial isoprene emissions using MEGAN (Model of Emissions of Gases and
626 Aerosols from Nature), Atmospheric Chemistry and Physics, 6, 3181-3210, 2006.

627 Guo, S., Hu, M., Zamora, M. L., Peng, J. F., Shang, D. J., Zheng, J., Du, Z. F., Wu, Z., Shao,
628 M., Zeng, L. M., Molina, M. J., and Zhang, R. Y.: Elucidating severe urban haze
629 formation in China, Proceedings of the National Academy of Sciences of the United
630 States of America, 111, 17373-17378, 10.1073/pnas.1419604111, 2014.

631 Guo, S., Hu, M., Wang, Z. B., Slanina, J., and Zhao, Y. L.: Size-resolved aerosol
632 water-soluble ionic compositions in the summer of Beijing: implication of regional
633 secondary formation, Atmospheric Chemistry and Physics, 10, 947-959, 2010.

634 Hong, S.-Y., and Lim, J.-O. J.: The WRF Single-Moment 6-Class Microphysics Scheme
635 (WSM6), Asia-Pacific Journal of Atmospheric Sciences, 42, 129-151, 2006.

636 Horowitz, L. W., Walters, S., Mauzerall, D. L., Emmons, L. K., Rasch, P. J., Granier, C., Tie,
637 X. X., Lamarque, J. F., Schultz, M. G., Tyndall, G. S., Orlando, J. J., and Brasseur, G. P.:
638 A global simulation of tropospheric ozone and related tracers: Description and evaluation
639 of MOZART, version 2, Journal of Geophysical Research-Atmospheres, 108, 29,
640 10.1029/2002jd002853, 2003.

641 Janjić, Z. I.: Nonsingular Implementation of the Mellor–Yamada Level 2.5 Scheme in the
642 NCEP Meso Model, Ncep Office Note, 436, 2002.

643 Jiang, C., Wang, H., Zhao, T., Li, T., and Che, H.: Modeling study of $PM_{2.5}$ pollutant
644 transport across cities in China's Jing-Jin-Ji region during a severe haze episode in
645 December 2013, Atmospheric Chemistry and Physics, 15, 5803-5814,
646 10.5194/acp-15-5803-2015, 2015.

647 Jiang, F., Wang, T. J., Wang, T. T., Xie, M., and Zhao, H.: Numerical modeling of a
648 continuous photochemical pollution episode in Hong Kong using WRF-Chem,
649 Atmospheric Environment, 42, 8717-8727, 10.1016/j.atmosenv.2008.08.034, 2008.

650 Kulmala, M., Laaksonen, A., and Pirjola, L.: Parameterizations for sulfuric acid/water
651 nucleation rates, Journal of Geophysical Research Atmosphere, 103, 8301– 8307, 1998.

652 Lang, J. L., Cheng, S. Y., Li, J. B., Chen, D. S., Zhou, Y., Wei, X., Han, L. H., and Wang, H.
653 Y.: A Monitoring and Modeling Study to Investigate Regional Transport and
654 Characteristics of $PM_{2.5}$ Pollution, Aerosol and Air Quality Research, 13, 943-956,
655 10.4209/aaqr.2012.09.0242, 2013.

656 Lei, W., de Foy, B., Zavala, M., Volkamer, R., and Molina, L. T.: Characterizing ozone
657 production in the Mexico City Metropolitan Area: a case study using a chemical transport
658 model, Atmospheric Chemistry and Physics, 7, 1347-1366, 2007.

659 Lei, W., Zavala, M., de Foy, B., Volkamer, R., and Molina, L. T.: Characterizing ozone
660 production and response under different meteorological conditions in Mexico City,
661 Atmospheric Chemistry and Physics, 8, 7571-7581, 2008.

662 Long, X., Tie, X., Cao, J., Huang, J., Feng, T., Li, N., Zhao, S., Tian, J., Li, G., and Zhang, Q.:
663 Impact of crop field burning and mountains on heavy haze in the North China Plain: a
664 case study, Atmospheric Chemistry and Physics, 16, 9675-9691,
665 doi:10.5194/acp-16-9675-2016, 2016.

666 Li, G., Zhang, R., Fan, J., and Tie, X.: Impacts of black carbon aerosol on photolysis and
667 ozone, Journal of Geophysical Research, 110, 10.1029/2005jd005898, 2005.

668 Li, G., Zhang, R., Fan, J., and Tie, X.: Impacts of biogenic emissions on photochemical
669 ozone production in Houston, Texas, Journal of Geophysical Research, 112,
670 10.1029/2006jd007924, 2007.

671 Li, G., Lei, W., Zavala, M., Volkamer, R., Dusanter, S., Stevens, P., and Molina, L. T.:
672 Impacts of HONO sources on the photochemistry in Mexico City during the
673 MCMA-2006/MILAGO Campaign, Atmospheric Chemistry and Physics, 10, 6551-6567,
674 10.5194/acp-10-6551-2010, 2010.

675 Li, G., Bei, N., Tie, X., and Molina, L. T.: Aerosol effects on the photochemistry in Mexico
676 City during MCMA-2006/MILAGRO campaign, Atmospheric Chemistry and Physics, 11,
677 5169-5182, 10.5194/acp-11-5169-2011, 2011a.

678 Li, G., Zavala, M., Lei, W., Tsimpidi, A. P., Karydis, V. A., Pandis, S. N., Canagaratna, M.
679 R., and Molina, L. T.: Simulations of organic aerosol concentrations in Mexico City using
680 the WRF-CHEM model during the MCMA-2006/MILAGRO campaign, Atmospheric
681 Chemistry and Physics, 11, 3789-3809, 10.5194/acp-11-3789-2011, 2011b.

682 Li, G., Lei, W., Bei, N., and Molina, L. T.: Contribution of garbage burning to chloride and
683 $PM_{2.5}$ in Mexico City, Atmospheric Chemistry and Physics, 12, 8751-8761,
684 10.5194/acp-12-8751-2012, 2012.

685 Li, G. H., Bei, N. F., Zavala, M., and Molina, L. T.: Ozone formation along the California
686 Mexican border region during Cal-Mex 2010 field campaign, Atmospheric Environment,
687 88, 370-389, 10.1016/j.atmosenv.2013.11.067, 2014.

688 Li, G., Bei, N., Cao, J., Huang, R., Wu, J., Feng, T., Wang, Y., Liu, S., Zhang, Q., Tie, X.,
689 and Molina, L.: A Possible Pathway for Rapid Growth of Sulfate during Haze Days in
690 China, Atmospheric Chemistry and Physics Discussion, 2016, 1-43,
691 10.5194/acp-2016-994, 2016.

692 Li, P., Yan, R., Yu, S., Wang, S., Liu, W., and Bao, H.: Reinstate regional transport of $PM_{2.5}$
693 as a major cause of severe haze in Beijing, Proceedings of the National Academy of
694 Sciences of the United States of America, 112, 2739-2740, 2015.

695 Li, R. K., Li, Z. P., Gao, W. J., Ding, W. J., Xu, Q., and Song, X. F.: Diurnal, seasonal, and
696 spatial variation of $PM_{2.5}$ in Beijing, Chinese Science Bulletin, 60, 387-395,
697 10.1007/s11434-014-0607-9, 2015a.

698 Liu, Z. R., Hu, B., Wang, L. L., Wu, F. K., Gao, W. K., and Wang, Y. S.: Seasonal and
699 diurnal variation in particulate matter (PM_{10} and $PM_{2.5}$) at an urban site of Beijing:
700 analyses from a 9-year study, Environmental Science and Pollution Research, 22,
701 627-642, 10.1007/s11356-014-3347-0, 2015.

Meng, W., Gao, Q., Zhang, Z., Liao, Q., Lei, t., Li, J., Kang, N., and Ren, Z.: The Numerical Study of Atmospheric Pollution in Beijing and Its Surrounding Regions, Research of Environmental Sciences, 19, 11-18, 2006.

Mlawer, E. J., Taubman, S. J., Brown, P. D., Iacono, M. J., and Clough, S. A.: Radiative transfer for inhomogeneous atmospheres: RRTM, a validated correlated-k model for the longwave, Journal of Geophysical Research-Atmospheres, 102, 16663-16682, 10.1029/97jd00237, 1997.

Molina, L. T. and Molina, M. J.: Air Quality in the Mexico Megacity: An Integrated Assessment, Kluwer Academic Publishers: Dordrecht, The Netherlands, 384 pp, 2002.

Molina, L. T., Kolb, C. E., de Foy, B., Lamb, B. K., Brune, W. H., Jimenez, J. L., Ramos-Villegas, R., Sarmiento, J., Paramo- Figueroa, V. H., Cardenas, B., Gutierrez-Avedoy, V., and Molina, M. J.: Air quality in North America's most populous city - overview of the MCMA-2003 campaign, Atmospheric Chemistry and Physics, 7, 2447–2473, doi: 10.5194/acp-7-2447-2007, 2007.

Molina, L. T., Madronich, S., Gaffney, J. S., Apel, E., de Foy, B., Fast, J., Ferrare, R., Herndon, S., Jimenez, J. L., Lamb, B., OsornioVargas, A. R., Russell, P., Schauer, J. J., Stevens, P. S., Volkamer, R., and Zavala, M.: An overview of the MILAGRO 2006 campaign: Mexico City emissions and their transport and transformation, Atmospheric Chemistry and Physics, 10, 8697–8760, doi: 10.5194/acp-10-8697-2010, 2010.

Nenes, A., Pilinis, C., Pandis, S. N.: ISORROPIA: A New thermodynamic equilibrium model for multiphase multicomponent inorganic aerosols, Aquatic Geochemistry, 4(1), 123-152, http://nenes.eas.gatech.edu/ISORROPIA/, 1998.

Parrish, D. and Zhu, T.: Clean air for Megacities, Science, 326, 674-675, 2009.

Parrish, D. D., and Stockwell, W. R.: Urbanization and Air Pollution: Then and Now, 96, 2015.

Peng, J. F., Hu, M., Guo, S., Du, Z. F., Zheng, J., Shang, D. J., Zamora, M. L., Zeng, L. M., Shao, M., Wu, Y. S., Zheng, J., Wang, Y., Glen, C. R., Collins, D. R., Molina, M. J., and Zhang, R. Y.: Markedly enhanced absorption and direct radiative forcing of black carbon under polluted urban environments, Proceedings of the National Academy of Sciences of the United States of America, 113, 4266-4271, 10.1073/pnas.1602310113, 2016.

Sillman, S., Logan, J. A., and Wofsy, S. C.: The sensitivity of ozone to nitrogen oxides and hydrocarbons in regional ozone episode, Journal of Geophysical Research-Atmospheres, 95, 1837-1851, 10.1029/JD095iD02p01837, 1990.

Stein, U., and Alpert, P.: Factor separation in numerical simulations, Journal of the Atmospheric Science, 50, 2107-2115, 10.1175/1520-0469(1993) 050<2107:fsins>2.0.co; 2, 1993.

Streets, D. G., Fu, J. S., Jang, C. J., Hao, J. M., He, K. B., Tang, X. Y., Zhang, Y. H., Wang, Z. F., Li, Z. P., Zhang, Q., Wang, L. T., Wang, B. Y., and Yu, C.: Air quality during the 2008 Beijing Olympic Games, Atmospheric Environment, 41, 480-492, 10.1016/j.atmosenv.2006.08.046, 2007.

Suarex, M. J., and Chou, M. D.: Technical report series on global modeling and data assimilation. Volume 3: An efficient thermal infrared radiation parameterization for use in general circulation models, 1603-1609, 1994.

Suh, I., Zhang, R. Y., Molina, L. T., and Molina, M. J.: Oxidation mechanism of aromatic peroxy and bicyclic radicals from OH-toluene reactions, Journal of American Chemical Society, 125, 12655-12665, 10.1021/ja0350280, 2003.

Sun, Y. L., Jiang, Q., Wang, Z. F., Fu, P. Q., Li, J., Yang, T., and Yin, Y.: Investigation of the sources and evolution processes of severe haze pollution in Beijing in January 2013, Journal of Geophysical Research-Atmospheres, 119, 4380-4398, 10.1002/2014jd021641, 2014.

Tang, G., Li, X., Wang, Y., Xin, J., and Ren, X.: Surface ozone trend details and interpretations in Beijing, 2001-2006, Atmospheric Chemistry and Physics, 9, 8813-8823, 2009.

Tang, G., Wang, Y., Li, X., Ji, D., Hsu, S., and Gao, X.: Spatial-temporal variations in surface ozone in Northern China as observed during 2009-2010 and possible implications for future air quality control strategies, Atmospheric Chemistry and Physics, 12, 2757-2776, 10.5194/acp-12-2757-2012, 2012.

Tang, G. Q., Zhang, J. Q., Zhu, X. W., Song, T., Munkel, C., Hu, B., Schafer, K., Liu, Z. R., Zhang, J. K., Wang, L. L., Xin, J. Y., Suppan, P., and Wang, Y. S.: Mixing layer height and its implications for air pollution over Beijing, China, Atmospheric Chemistry and Physics, 16, 2459-2475, 10.5194/acp-16-2459-2016, 2016.

Tao, M. H., Chen, L. F., Xiong, X. Z., Zhang, M. G., Ma, P. F., Tao, J. H., and Wang, Z. F.: Formation process of the widespread extreme haze pollution over northern China in January 2013: Implications for regional air quality and climate, Atmospheric Environment, 98, 417-425, 10.1016/j.atmosenv.2014.09.026, 2014.

Volkamer, R., San Martini, F., Molina, L. T., Salcedo, D., Jimenez, J. L., and Molina, M. J.: A Missing Sink for Gas-Phase Glyoxal in Mexico City: Formation of Secondary Organic Aerosol, Geophysical Research Letter, 34, L19807, doi:10.1029/2007GL030752, 2007.

Wang, H., Xue, M., Zhang, X. Y., Liu, H. L., Zhou, C. H., Tan, S. C., Che, H. Z., Chen, B., and Li, T.: Mesoscale modeling study of the interactions between aerosols and PBL meteorology during a haze episode in Jing-Jin-Ji (China) and its nearby surrounding region - Part 1: Aerosol distributions and meteorological features, Atmospheric Chemistry and Physics, 15, 3257-3275, 10.5194/acp-15-3257-2015, 2015.

Wang, L. L., Liu, Z. R., Sun, Y., Ji, D. S., and Wang, Y. S.: Long-range transport and regional sources of $PM_{2.5}$ in Beijing based on long-term observations from 2005 to 2010, Atmospheric Research, 157, 37-48, 10.1016/j.atmosres.2014.12.003, 2015.

Wang, L. T., Wei, Z., Yang, J., Zhang, Y., Zhang, F. F., Su, J., Meng, C. C., and Zhang, Q.: The 2013 severe haze over southern Hebei, China: model evaluation, source apportionment, and policy implications, Atmospheric Chemistry and Physics, 14, 3151-3173, 10.5194/acp-14-3151-2014, 2014a.

Wang, X. S., Li, J. L., Zhang, Y. H., Xie, S. D., and Tang, X. Y.: Ozone source attribution during a severe photochemical smog episode in Beijing, China, Science China Chemistry, 52, 1270-1280, 10.1007/s11426-009-0137-5, 2009.

Wang, Y., Khalizov, A., Levy, M., and Zhang, R. Y.: New Directions: Light absorbing aerosols and their atmospheric impacts, Atmospheric Environment, 81, 713-715, 10.1016/j.atmosenv.2013.09.034, 2013.

Wang, Y., Konopka, P., Liu, Y., Chen, H., Muller, R., Ploger, F., Riese, M., Cai, Z., and Lu, D.: Tropospheric ozone trend over Beijing from 2002-2010: ozonesonde measurements and modeling analysis, Atmospheric Chemistry and Physics, 12, 8389-8399, 10.5194/acp-12-8389-2012, 2012.

Wang, Y. H., Hu, B., Tang, G. Q., Ji, D. S., Zhang, H. X., Bai, J. H., Wang, X. K., and Wang, Y. S.: Characteristics of ozone and its precursors in Northern China: A comparative study of three sites, Atmospheric Research, 132, 450-459, 10.1016/j.atmosres.2013.04.005, 2013.

Wang, Z., Li, Y., Chen, T., Zhang, D., Sun, F., Wang, X., Huan, N., and Pan, L.: Analysis on diurnal variation characteristics of ozone and correlations with its precursors in urban atmosphere of Beijing, China Environmental Science, 34, 3001-3008, 2014b.

Wang, Z., Zhang, D., Li, Y., Dong, X., Sun, R., and Sun, N.: Different Air Pollution Situations of O_3 and $PM_{2.5}$ During Summer in Beijing, Environmental Science, 37, 807-815, 2016.

Wang, Z. F., Li-Na, L. I., Qi-Zhong, W. U., Gao, C., Xin, L. I., Student, G., and PhD: Simulation of the Impacts of Regional Transport on Summer Ozone Levels Over Beijing, Chinese Journal of Nature, 2008.

Weinroth, E., Luria, M., Emery, C., Ben-Nun, A., Bornstein, R., Kaplan, J., Peleg, M., and Mahrer, Y.: Simulations of Mideast transboundary ozone transport: A source apportionment case study, Atmospheric Environment, 42, 3700-3716, 10.1016/j.atmosenv.2008.01.002, 2008.

Wesely, M. L.: Parameterization of surface resistances to gaseous dry deposition in regional-scale numerical models, Atmospheric Environment, 23, 1293-1304, 10.1016/0004-6981(89)90153-4, 1989.

Xie, Y. Y., Wang, Y. X., Zhang, K., Dong, W. H., Lv, B. L., and Bai, Y. Q.: Daily Estimation of Ground-Level $PM_{2.5}$ Concentrations over Beijing Using 3 km Resolution MODIS AOD, Environmental Science & Technology, 49, 12280-12288, 10.1021/acs.est.5b01413, 2015.

Yang, T., Wang, Z. F., Zhang, B., Wang, X. Q., Wang, W., Gbauidi, A., and Gong, Y. B.: Evaluation of the effect of air pollution control during the Beijing 2008 Olympic Games using Lidar data, Chinese Science Bulletin, 55, 1311-1316, 10.1007/s11434-010-0081-y, 2010.

Zhang, L., Liao, H., and Li, J. P.: Impacts of Asian summer monsoon on seasonal and interannual variations of aerosols over eastern China, Journal of Geophysical

822 Research-Atmospheres, 115, 20, 10.1029/2009jd012299, 2010.

823 Zhang, J. P., Zhu, T., Zhang, Q. H., Li, C. C., Shu, H. L., Ying, Y., Dai, Z. P., Wang, X., Liu,
824 X. Y., Liang, A. M., Shen, H. X., and Yi, B. Q.: The impact of circulation patterns on
825 regional transport pathways and air quality over Beijing and its surroundings,
826 Atmospheric Chemistry and Physics, 12, 5031-5053, 10.5194/acp-12-5031-2012, 2012.

827 Zhang, Q., Streets, D. G., Carmichael, G. R., He, K. B., Huo, H., Kannari, A., Klimont, Z.,
828 Park, I. S., Reddy, S., Fu, J. S., Chen, D., Duan, L., Lei, Y., Wang, L. T., and Yao, Z. L.:
829 Asian emissions in 2006 for the NASA INTEX-B mission, Atmospheric Chemistry and
830 Physics, 9, 5131-5153, 2009.

831 Zhang, Q., Yuan, B., Shao, M., Wang, X., Lu, S., Lu, K., Wang, M., Chen, L., Chang, C. C.,
832 and Liu, S. C.: Variations of ground-level O_3 and its precursors in Beijing in summertime
833 between 2005 and 2011, Atmospheric Chemistry and Physics, 14, 6089-6101,
834 10.5194/acp-14-6089-2014, 2014.

835 Zhang, R., Guo, S., Levy, Z. M., and Hu, M.: Reply to Li et al.: Insufficient evidence for the
836 contribution of regional transport to severe haze formation in Beijing, Proceedings of the
837 National Academy of Sciences of the United States of America , 112, 201503855, 2015.

838 Zhang, R., Jing, J., Tao, J., Hsu, S.-C., Wang, G., Cao, J., Lee, C. S. L., Zhu, L., Chen, Z.,
839 Zhao, Y., and Shen, Z.: Chemical characterization and source apportionment of $PM_{2.5}$ in
840 Beijing: seasonal perspective, Atmospheric Chemistry and Physics, 13, 7053-7074,
841 doi:10.5194/acp-13-7053-2013, 2013.

842 Zhang, R., Wang, L., Khalizova, A. F., Zhao, J., Zheng, J., Mc-Grawb, R. L., and Molina, L.
843 T.: Formation of nanoparticles of blue haze enhanced by anthropogenic pollution,
844 Proceedings of the National Academy of Sciences of the United States of America, 106,
845 17650–17654, 2009.

846 Zhang, R., Khalizova, A. F., Wang, L., Hu, M., and Xu, W.: Nucleation and growth of
847 nanoparticles in the atmosphere, Chemical Reviews. 112, 1957–2011, 2012.

848 Zhang, R. Y., Wang, G. H., Guo, S., Zarnora, M. L., Ying, Q., Lin, Y., Wang, W. G., Hu, M.,
849 and Wang, Y.: Formation of Urban Fine Particulate Matter, Chemical Reviews, 115,
850 3803-3855, 10.1021/acs.chemrev.5b00067, 2015.

851 Zhao, C., Wang, Y., and Zeng, T.: East China plains: a "basin" of ozone pollution,
852 Environmental Science & Technology, 43, 1911-1915, 2009.

853 Zhao, J., Levitt, N. P., Zhang, R. Y., and Chen, J. M.: Heterogeneous reactions of
854 methylglyoxal in acidic media: implications for secondary organic aerosol formation,
855 Environment Science & Technology., 40, 7682–7687, 2006.

856 Zheng, S., Pozzer, A., Cao, C. X., and Lelieveld, J.: Long-term (2001-2012) concentrations
857 of fine particulate matter ($PM_{2.5}$) and the impact on human health in Beijing, China,
858 Atmospheric Chemistry and Physics, 15, 5715-5725, 10.5194/acp-15-5715-2015, 2015.
859

860

Table 1 Emissions of major anthropogenic species in July 2013 (Unit: 10^6 g $month^{-1}$)

Region	VOC	NO_x	OC	SO_2	CO	$PM_{2.5}$
Beijing Municipality	29303	26272	976	8796	119254	5319
Tianjin Municipality	29255	34534	1424	23204	181940	8831
Hebei Province	101710	190352	12732	136957	1239510	67877
Shanxi Province	35933	93069	6381	131758	355823	36473
Shandong Province	246538	235485	12181	246538	937528	77681

869 Table 2 Hourly mass concentrations of pollutants averaged in the afternoon at 12
870 monitoring sites in Beijing during summertime of 2013 and 2015.

Pollutants	CO (mg m^{-3})	SO_2 (μg m^{-3})	NO_2 (μg m^{-3})	O_3 (μg m^{-3})	$PM_{2.5}$ (μg m^{-3})
2013	1.09	9.85	31.6	133.0	81.4
2015	0.88	5.71	23.6	163.2	61.9
Change (%)	-20.0	-42.0	-25.1	+22.8	-24.0

871
872
873
874
875

Table 3 Average O_3 contributions (%) from 12:00 to 18:00 BJT in Beijing from local emissions, non-Beijing emissions, the interactions of both emissions, and background from 5 to 14 July 2015.

Emissions	Beijing	Surroundings	Interactions	Background
Date	f'_B	f'_S	f'_{BS}	f_0
5	15.5	26.1	-2.4	60.8
6	19.8	30.9	-3.0	52.3
7	25.5	36.0	-3.6	42.1
8	27.0	36.9	-5.9	42.0
9	23.2	35.3	-4.6	46.1
10	18.6	39.9	-2.6	44.1
11	29.4	48.0	-10.0	32.6
12	35.4	40.6	-11.4	35.4
13	23.4	15.2	-1.5	62.9
14	20.3	32.2	-3.3	50.8
Average	22.4	36.6	-5.1	46.1

883 Table 4 Average $PM_{2.5}$ contributions (%) in Beijing from local emissions, non-Beijing
884 emissions, the interactions of both emissions, and background from 5 to 14 July 2015.
885

Emissions	Beijing	Surroundings	Interactions	Background
Date	f'_B	f'_S	f'_{BS}	f_0
5	14.6	55.1	3.3	27.0
6	14.9	56.3	3.4	25.4
7	14.2	56.4	8.0	21.4
8	13.2	61.1	6.4	19.3
9	15.3	61.3	6.3	17.1
10	11.5	66.5	6.2	15.8
11	9.7	71.0	8.1	11.2
12	14.2	67.6	5.6	12.6
13	19.2	47.2	3.6	30.0
14	16.6	53.1	6.4	23.9
Average	13.7	61.5	5.9	18.9

886
887
888
889

890 Table 5 Aerosol species' contributions (%) from local emissions, non-Beijing emissions,
891 interactions of both emissions, and background, and mass fraction in the total $PM_{2.5}$ (%) in
892 Beijing averaged during the period from 5 to 14 July 2015.
893

Emissions Species	Mass Fraction In Total $PM_{2.5}$	Beijing f'_B	Surroundings f'_S	Interactions f'_{BS}	Background f_0
EC	5.8	27.0	57.9	1.5	13.6
POA	9.8	20.8	49.0	5.3	24.9
SOA	25.0	14.6	64.2	5.9	15.3
Ammonium	13.7	14.5	65.7	1.5	18.3
Nitrate	14.1	10.1	71.7	18.1	0.1
Sulfate	25.1	6.5	52.9	3.4	37.2
Unspecified	6.5	21.2	61.4	1.6	15.8

894
895
896
897

Figure Captions

Figure 1 WRF-CHEM simulation domain. The blue circles represent centers of cities with ambient monitoring sites and the red circle denotes the NCNST site. The size of the blue circle denotes the number of ambient monitoring sites of cities.

Figure 2 Spatial distribution of anthropogenic (a) NO_x (b) VOC_s (c) OC (d) SO_2 emission rates (g $month^{-1}$) in the simulation domain.

Figure 3 Comparison of measured (black dots) and predicted (blue line) diurnal profiles of near-surface hourly (a) $PM_{2.5}$, (b) O_3, and (c) NO_2 averaged over all ambient monitoring stations in Beijing from 5 to 14 July 2015.

Figure 4 Comparison of measured (black dots) and simulated (black line) diurnal profiles of submicron aerosol species of (a) POA, (b) SOA, (c) sulfate, (d) nitrate, and (e) ammonium at NCNST site in Beijing from 5 to 14 July 2015.

Figure 5 Comparison of measured (black dots) and predicted (blue line) diurnal profiles of near-surface hourly (a) $PM_{2.5}$, (b) O_3, and (c) NO_2 averaged over all ambient monitoring stations in BTH from 5 to 14 July 2015.

Figure 6 Pattern comparison of simulated vs. observed near-surface $PM_{2.5}$ at 10:00 BJT during the selected periods from 5 to 14 July 2015. Colored circles: $PM_{2.5}$ observations; color contour: $PM_{2.5}$ simulations; black arrows: simulated surface winds.

Figure 7 Same as Figure 6, but for O_3 at 15:00 BJT.

Figure 8 Same as Figure 6, but for NO_2 at 08:00 BJT.

Figure 9 Temporal variations of total net horizontal transport flux of $PM_{2.5}$, O_3 and NO_2 over Beijing boundary (blue line) and the contribution of non-Beijing emission to the $PM_{2.5}$, O_3 and NO_2 concentrations in Beijing (black line) during the study episode.

Figure 10 Temporal variations of the average near-surface O_3 and $PM_{2.5}$ concentrations from $\boldsymbol{f_{BS}}$ with all the emissions (black line), $\boldsymbol{f_B}$ with Beijing emissions alone (blue line), and $\boldsymbol{f_S}$ with non-Beijing emissions alone (red line) in Beijing from 5 to 14 July 2015.

Figure 11 Temporal variations of the average contributions to the near-surface aerosol species concentrations from total emissions (black line, defined as $\boldsymbol{f_{BS}}$), local emissions (blue line, $\boldsymbol{f'_B}$, defined as $\boldsymbol{f_B - f_0}$), non-Beijing emissions (red line, $\boldsymbol{f'_S}$, defined as $\boldsymbol{f_S - f_0}$), the emission interactions (green line, $\boldsymbol{f'_{BS}}$, defined as $\boldsymbol{f_{BS} - f_B - f_S + f_0}$), and background (black dashed line, defined as $\boldsymbol{f_0}$) in

Beijing from 5 to 14 July 2015.

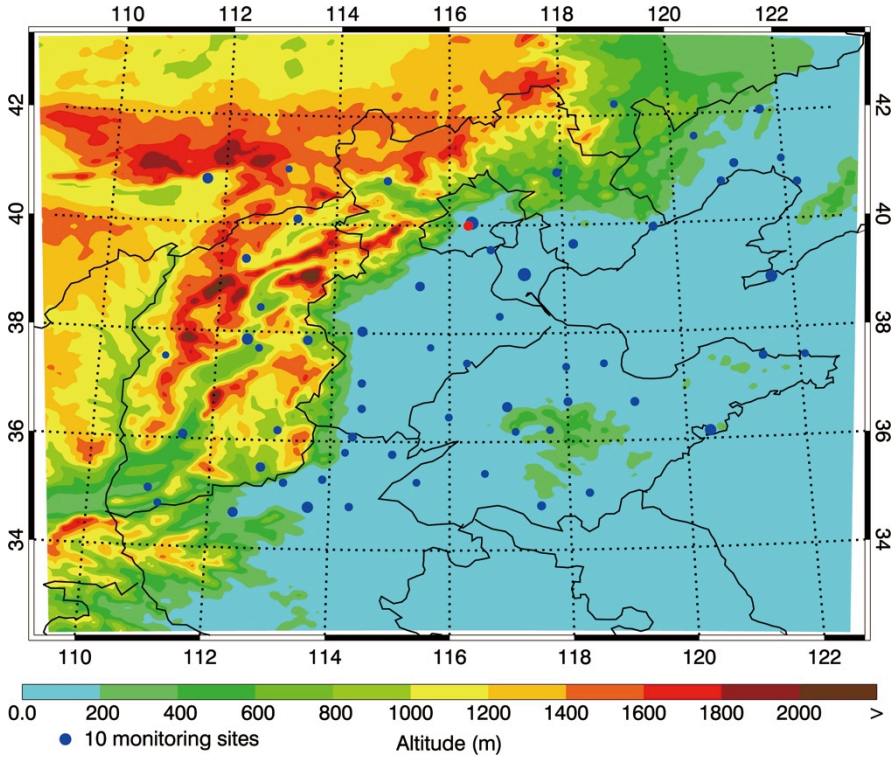
110
112
114
116
118
120
122
42
40
38
36
34
0.0
200
400
600
800
1000
1200
1400
1600
1800
2000
>
10 monitoring sites
Altitude (m)

Figure 1

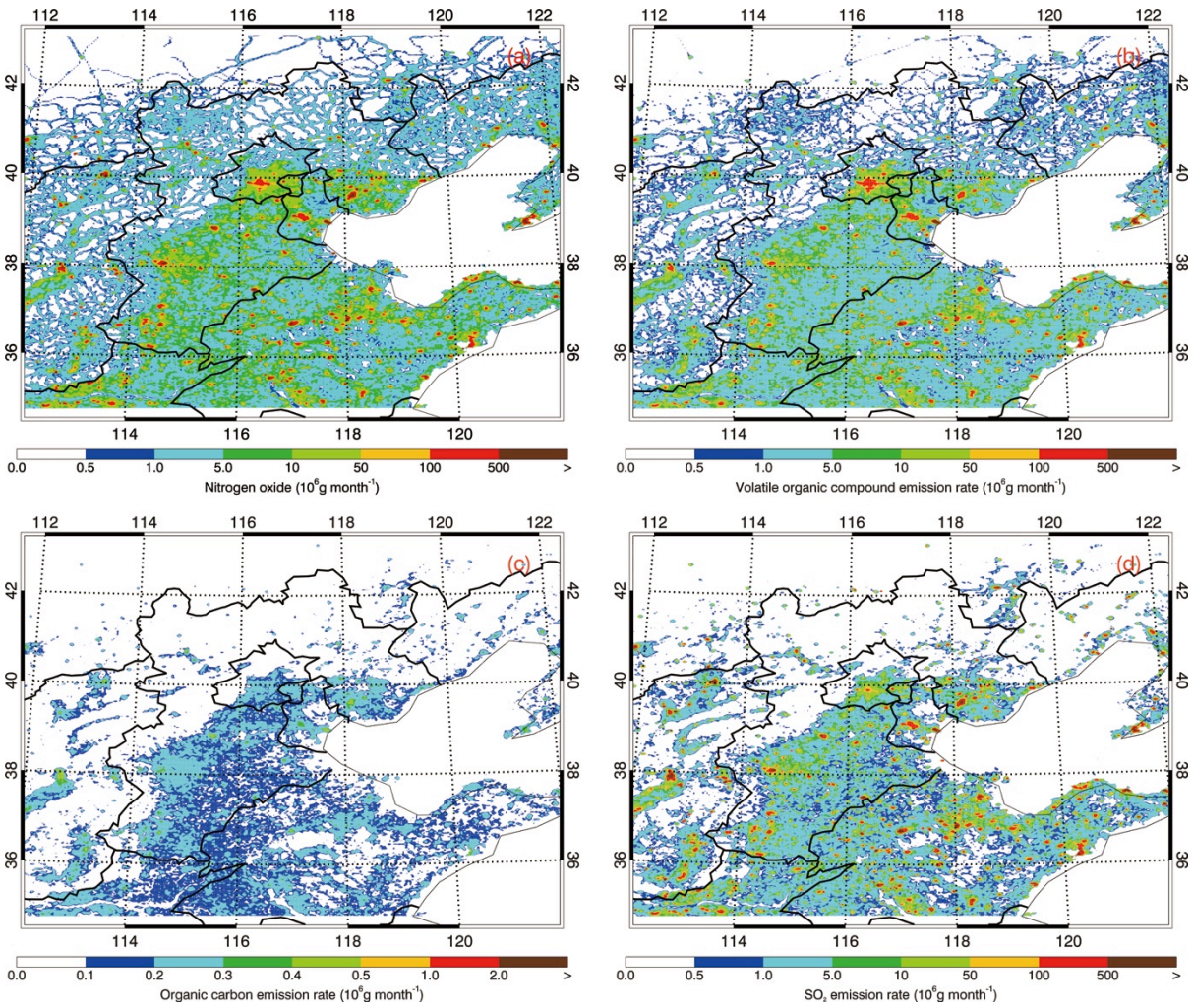
(a)
(b)
(c)
(d)
112 114 116 118 120 122
42 40 38 36
0.0 0.5 1.0 5.0 10 50 100 500 >
Nitrogen oxide (10^6g month^{-1})
Volatile organic compound emission rate (10^6g month^{-1})
0.0 0.1 0.2 0.3 0.4 0.5 1.0 2.0 >
Organic carbon emission rate (10^6g month^{-1})
SO_2 emission rate (10^6g month^{-1})

Figure 2

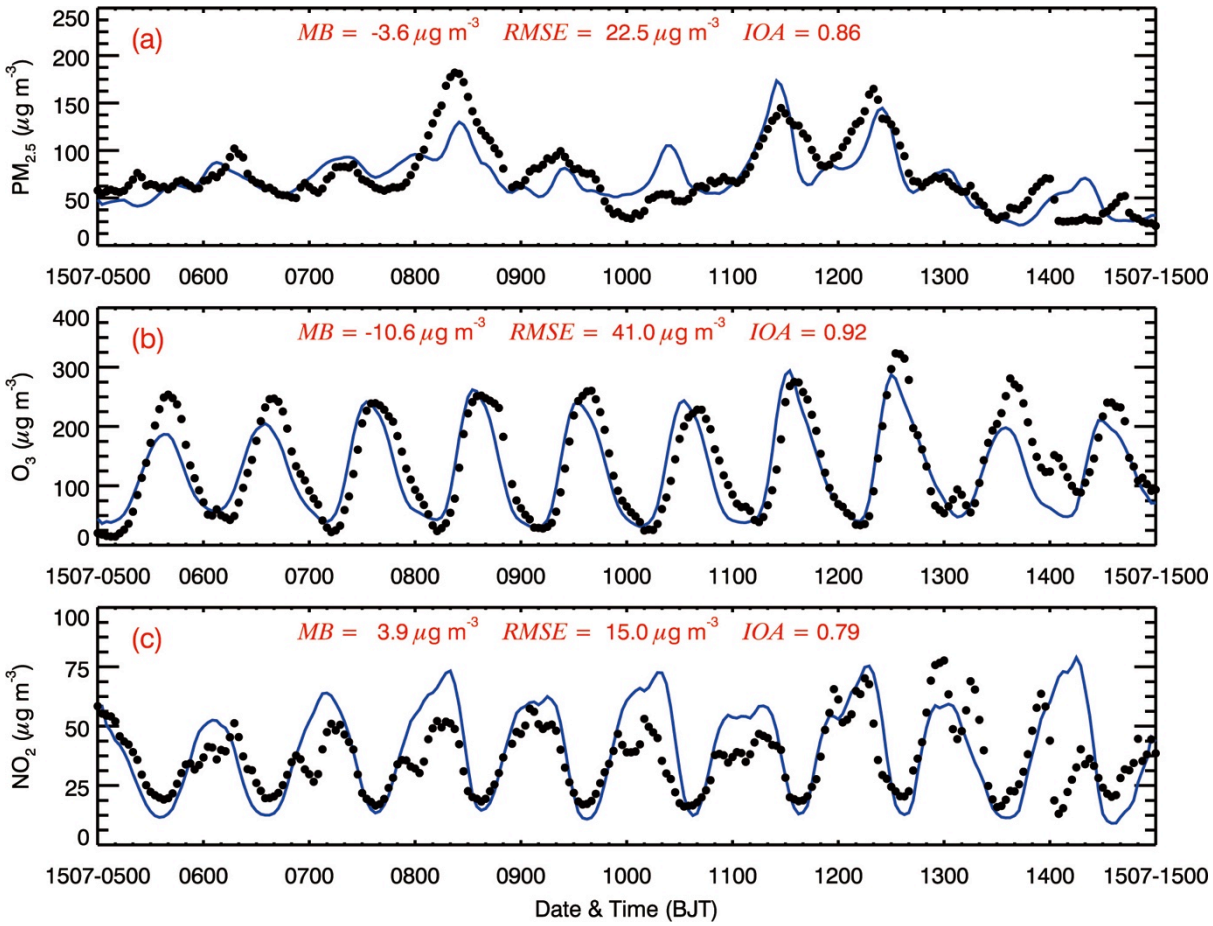
(a)
MB = -3.6 μg m-3 RMSE = 22.5 μg m-3 IOA = 0.86
PM2.5 (μg m-3)
(b)
MB = -10.6 μg m-3 RMSE = 41.0 μg m-3 IOA = 0.92
O3 (μg m-3)
(c)
MB = 3.9 μg m-3 RMSE = 15.0 μg m-3 IOA = 0.79
NO2 (μg m-3)
1507-0500 0600 0700 0800 0900 1000 1100 1200 1300 1400 1507-1500
Date & Time (BJT)

Figure 3

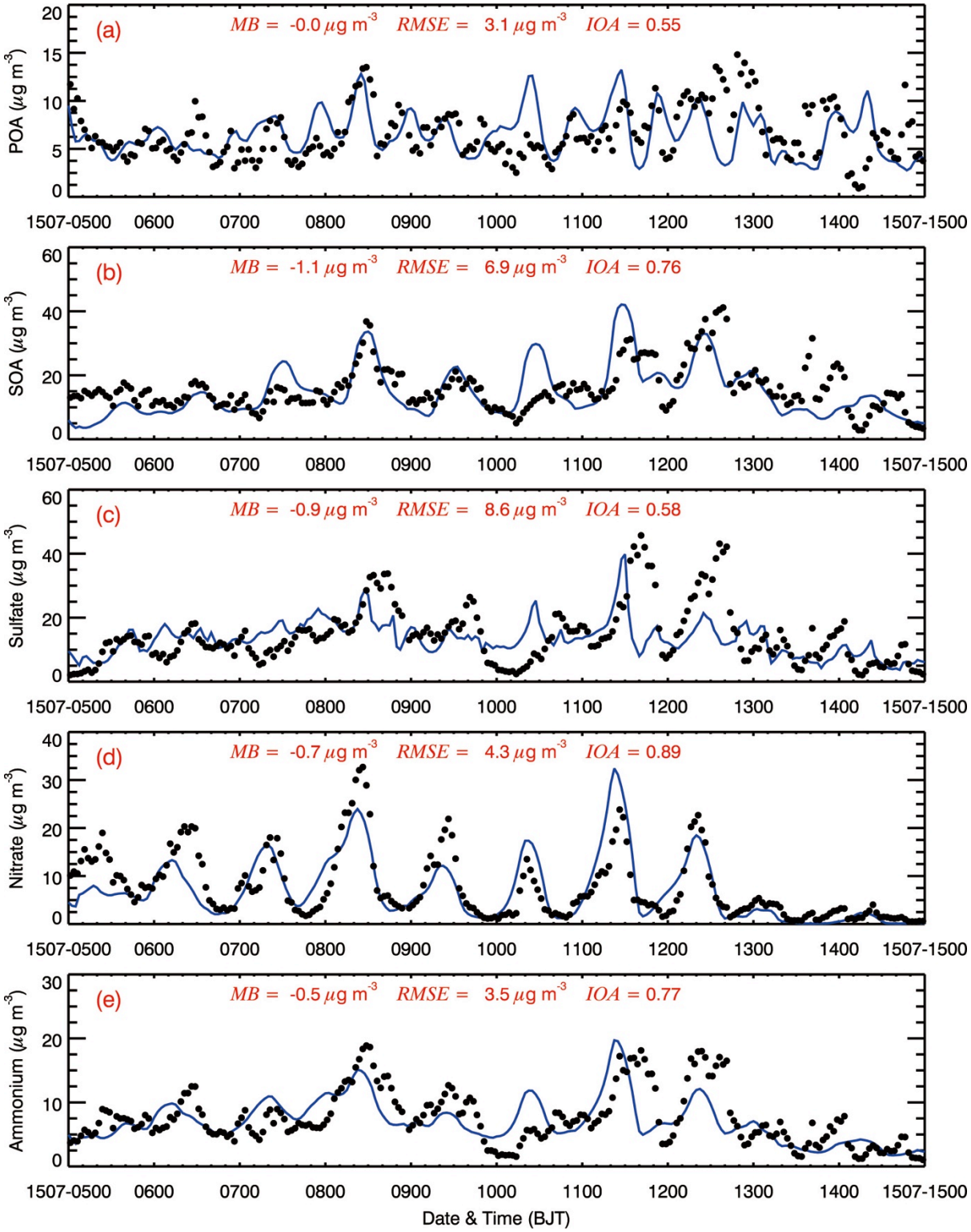
(a)
MB = -0.0 μg m-3 RMSE = 3.1 μg m-3 IOA = 0.55
POA (μg m-3)
(b)
MB = -1.1 μg m-3 RMSE = 6.9 μg m-3 IOA = 0.76
SOA (μg m-3)
(c)
MB = -0.9 μg m-3 RMSE = 8.6 μg m-3 IOA = 0.58
Sulfate (μg m-3)
(d)
MB = -0.7 μg m-3 RMSE = 4.3 μg m-3 IOA = 0.89
Nitrate (μg m-3)
(e)
MB = -0.5 μg m-3 RMSE = 3.5 μg m-3 IOA = 0.77
Ammonium (μg m-3)
1507-0500 0600 0700 0800 0900 1000 1100 1200 1300 1400 1507-1500
Date & Time (BJT)

Figure 4

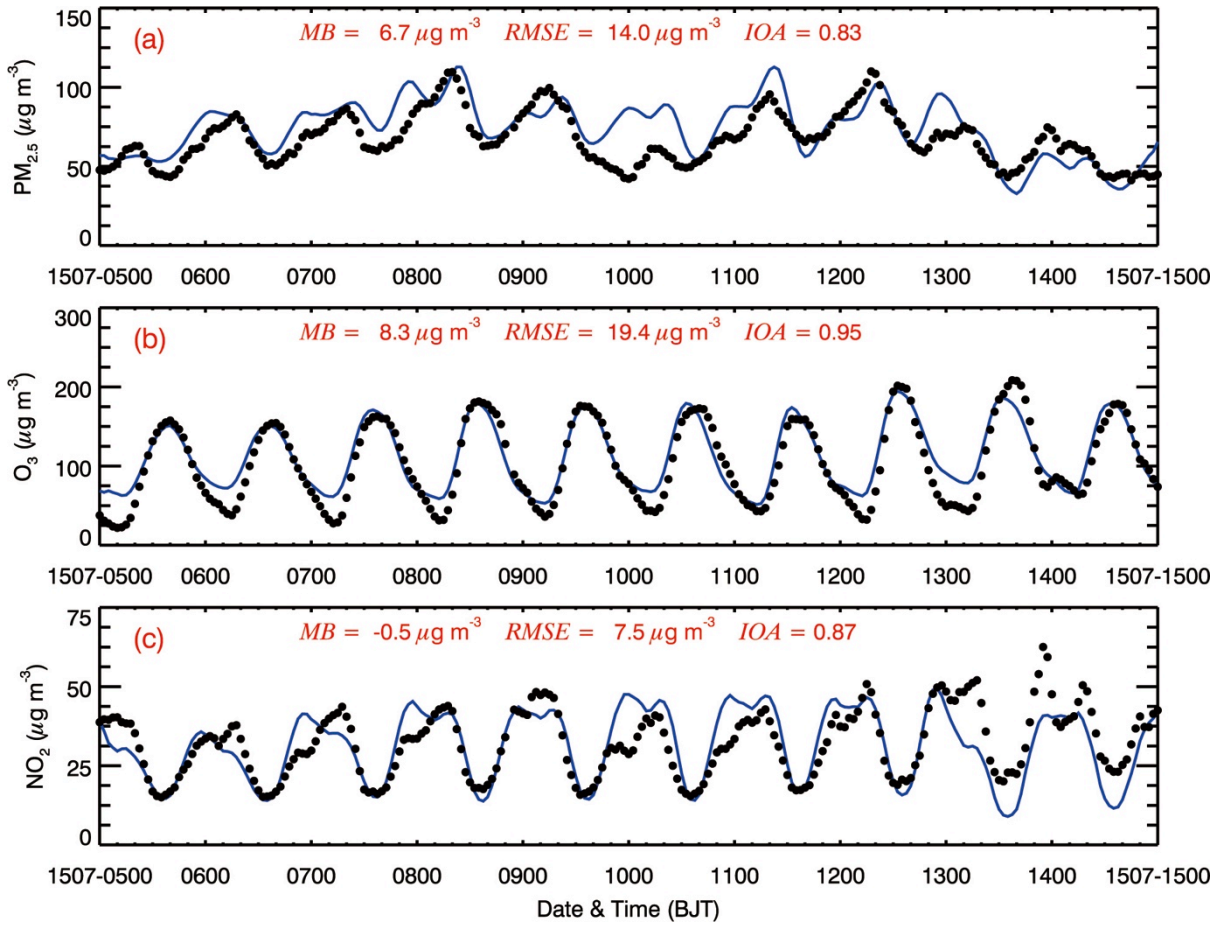
(a)
MB = 6.7 μg m-3 RMSE = 14.0 μg m-3 IOA = 0.83
PM2.5 (μg m-3)
(b)
MB = 8.3 μg m-3 RMSE = 19.4 μg m-3 IOA = 0.95
O3 (μg m-3)
(c)
MB = -0.5 μg m-3 RMSE = 7.5 μg m-3 IOA = 0.87
NO2 (μg m-3)
1507-0500 0600 0700 0800 0900 1000 1100 1200 1300 1400 1507-1500
Date & Time (BJT)

Figure 5

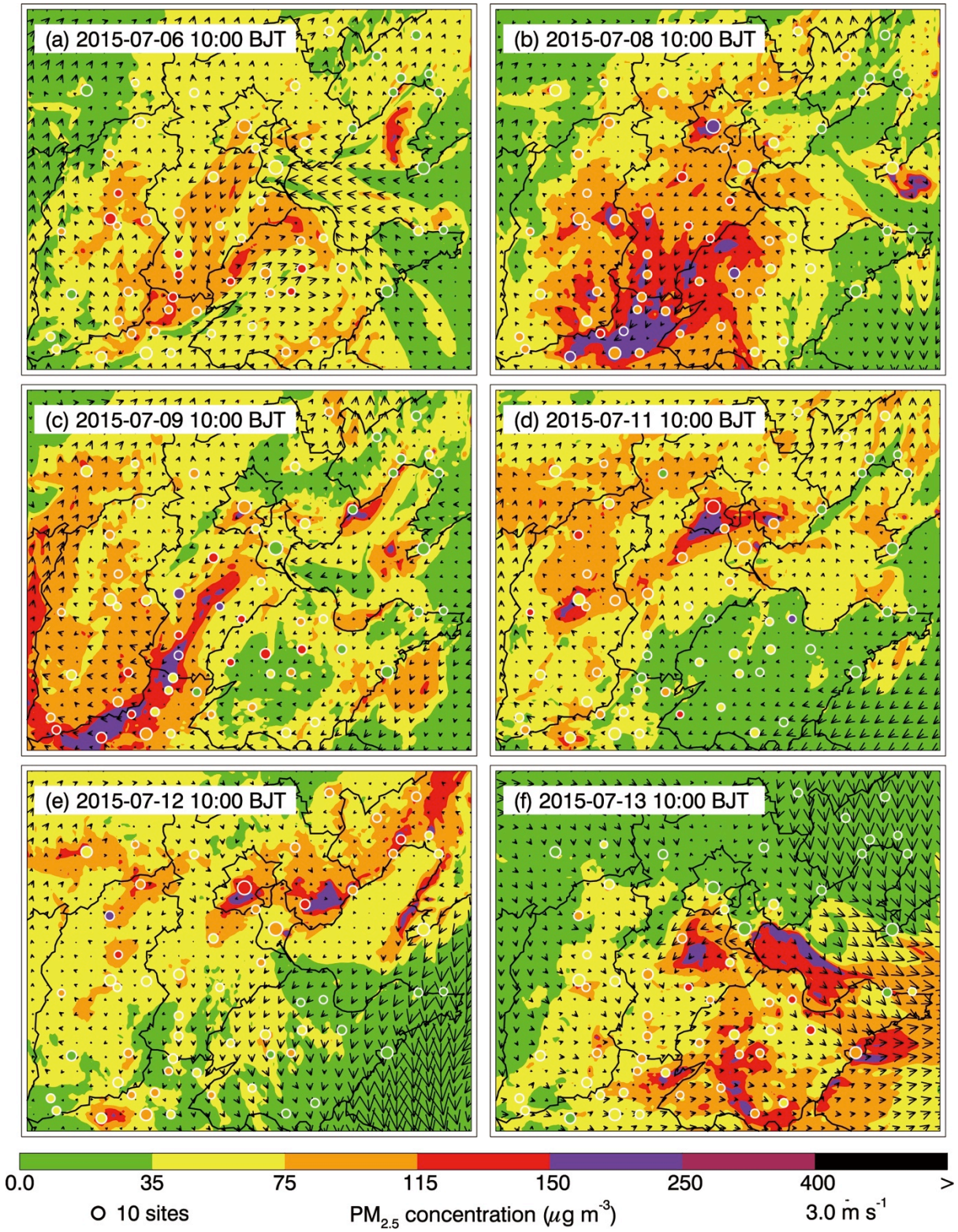
(a) 2015-07-06 10:00 BJT
(b) 2015-07-08 10:00 BJT
(c) 2015-07-09 10:00 BJT
(d) 2015-07-11 10:00 BJT
(e) 2015-07-12 10:00 BJT
(f) 2015-07-13 10:00 BJT
0.0
35
75
115
150
250
400
>
10 sites
PM2.5 concentration (μg m-3)
3.0 m s-1

Figure 6

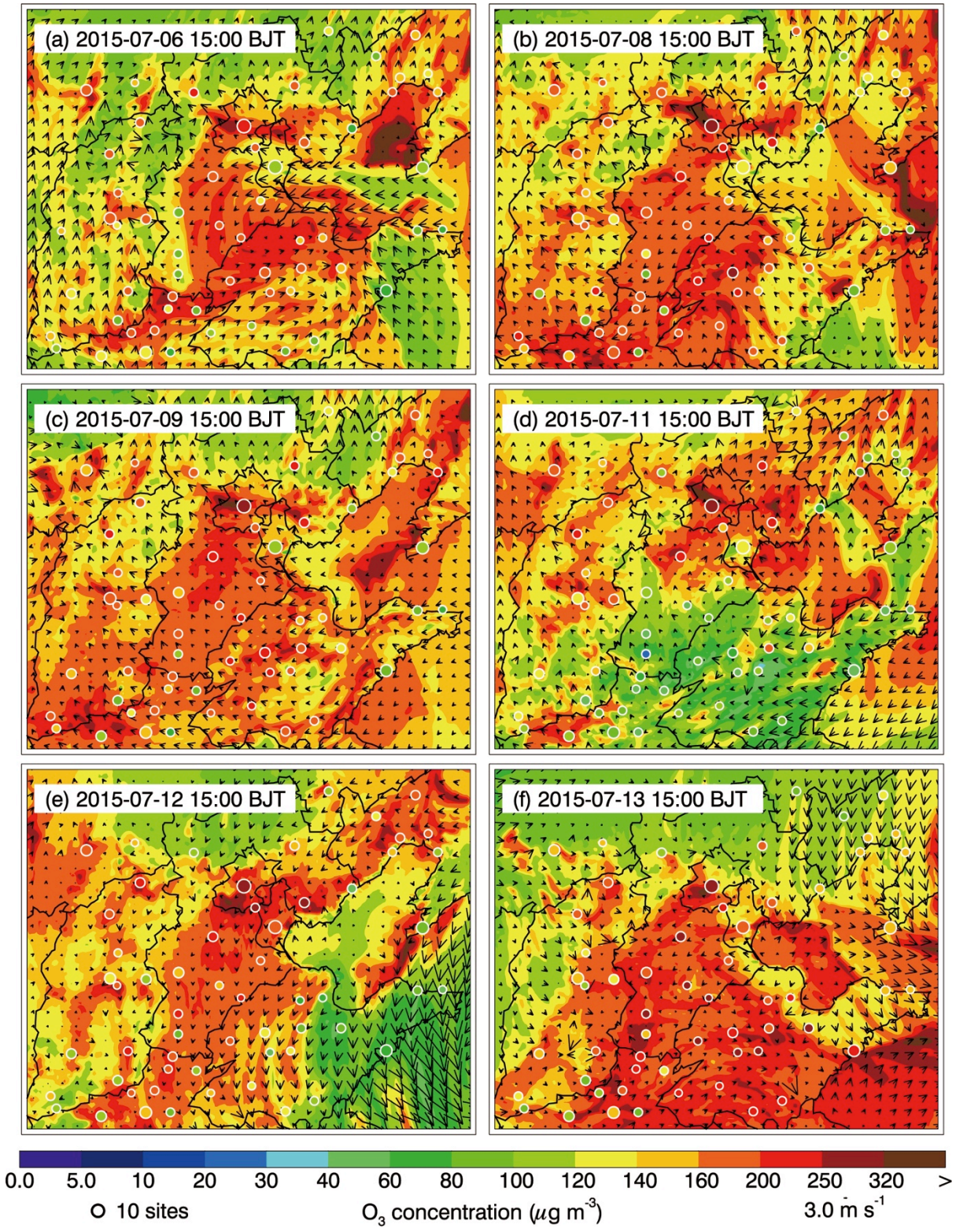
(a) 2015-07-06 15:00 BJT
(b) 2015-07-08 15:00 BJT
(c) 2015-07-09 15:00 BJT
(d) 2015-07-11 15:00 BJT
(e) 2015-07-12 15:00 BJT
(f) 2015-07-13 15:00 BJT
0.0 5.0 10 20 30 40 60 80 100 120 140 160 200 250 320 >
O 10 sites
O3 concentration (μg m-3)
3.0 m s-1

Figure 7

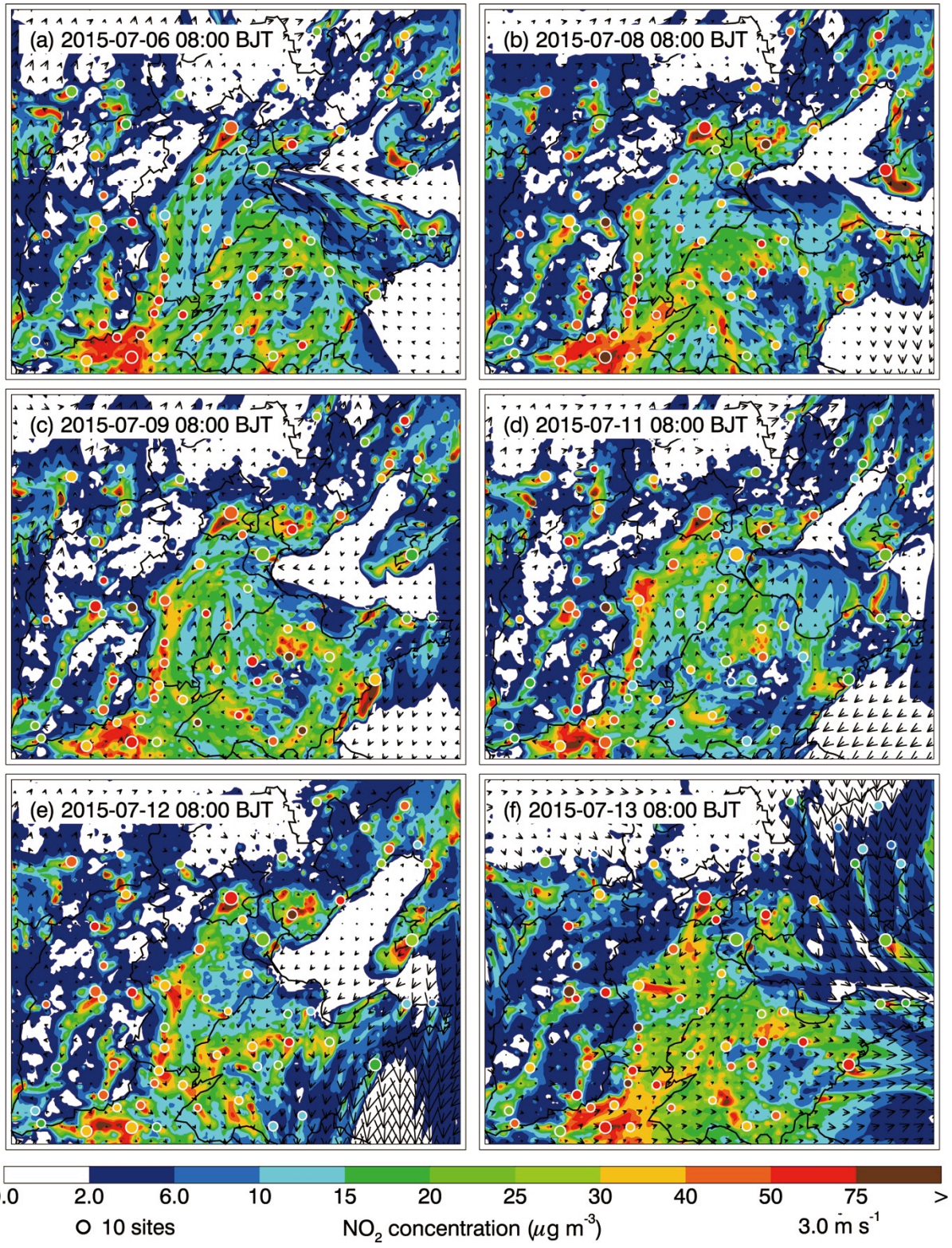
(a) 2015-07-06 08:00 BJT
(b) 2015-07-08 08:00 BJT
(c) 2015-07-09 08:00 BJT
(d) 2015-07-11 08:00 BJT
(e) 2015-07-12 08:00 BJT
(f) 2015-07-13 08:00 BJT
0.0
2.0
6.0
10
15
20
25
30
40
50
75
>
O 10 sites
NO2 concentration (μg m-3)
3.0 m s-1

Figure 8

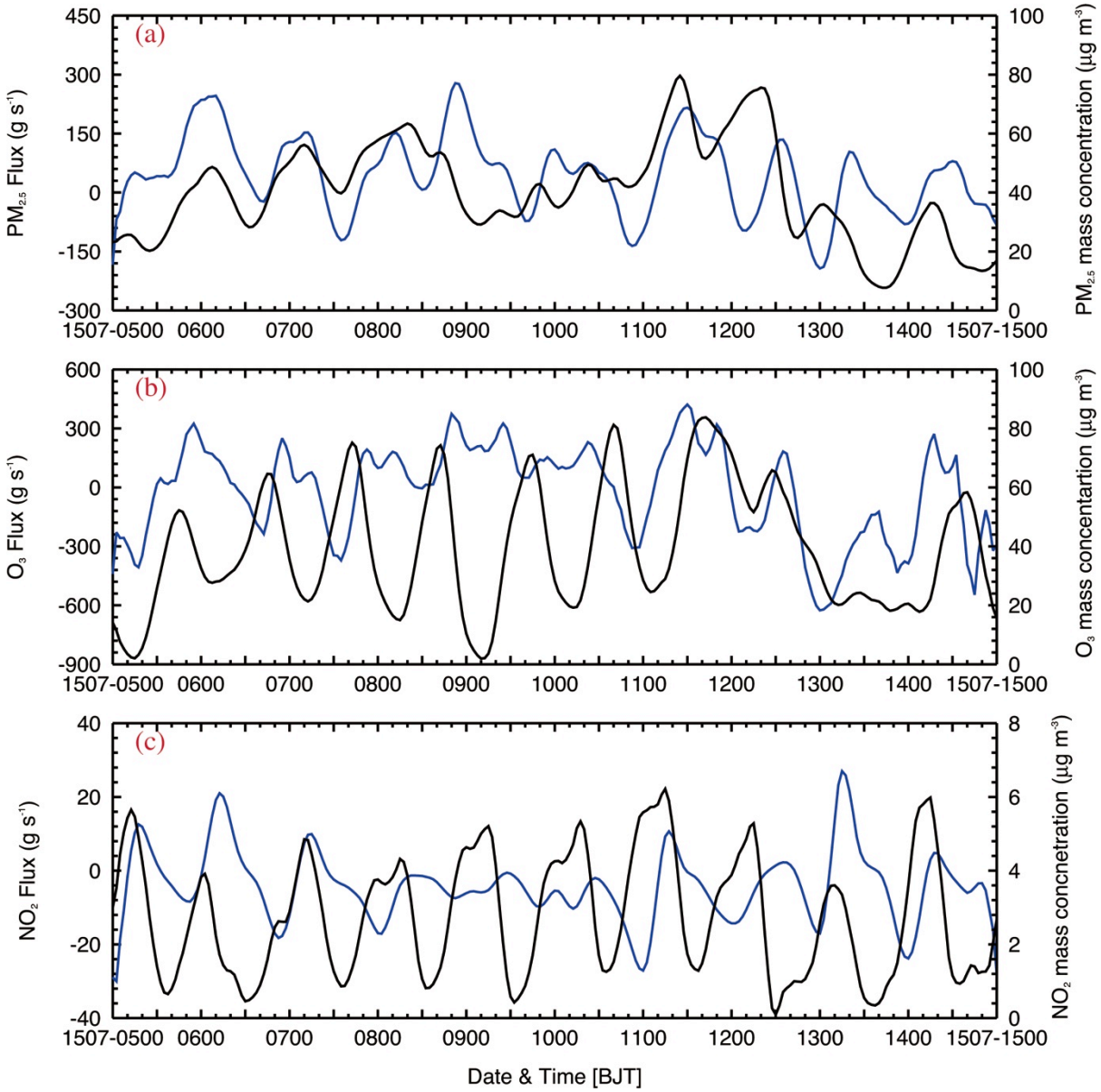
(a)
(b)
(c)
PM2.5 Flux (g s-1)
PM2.5 mass concentration (μg m-3)
O3 Flux (g s-1)
O3 mass concentartion (μg m-3)
NO2 Flux (g s-1)
NO2 mass concnetration (μg m-3)
1507-0500 0600 0700 0800 0900 1000 1100 1200 1300 1400 1507-1500
Date & Time [BJT]

Figure 9

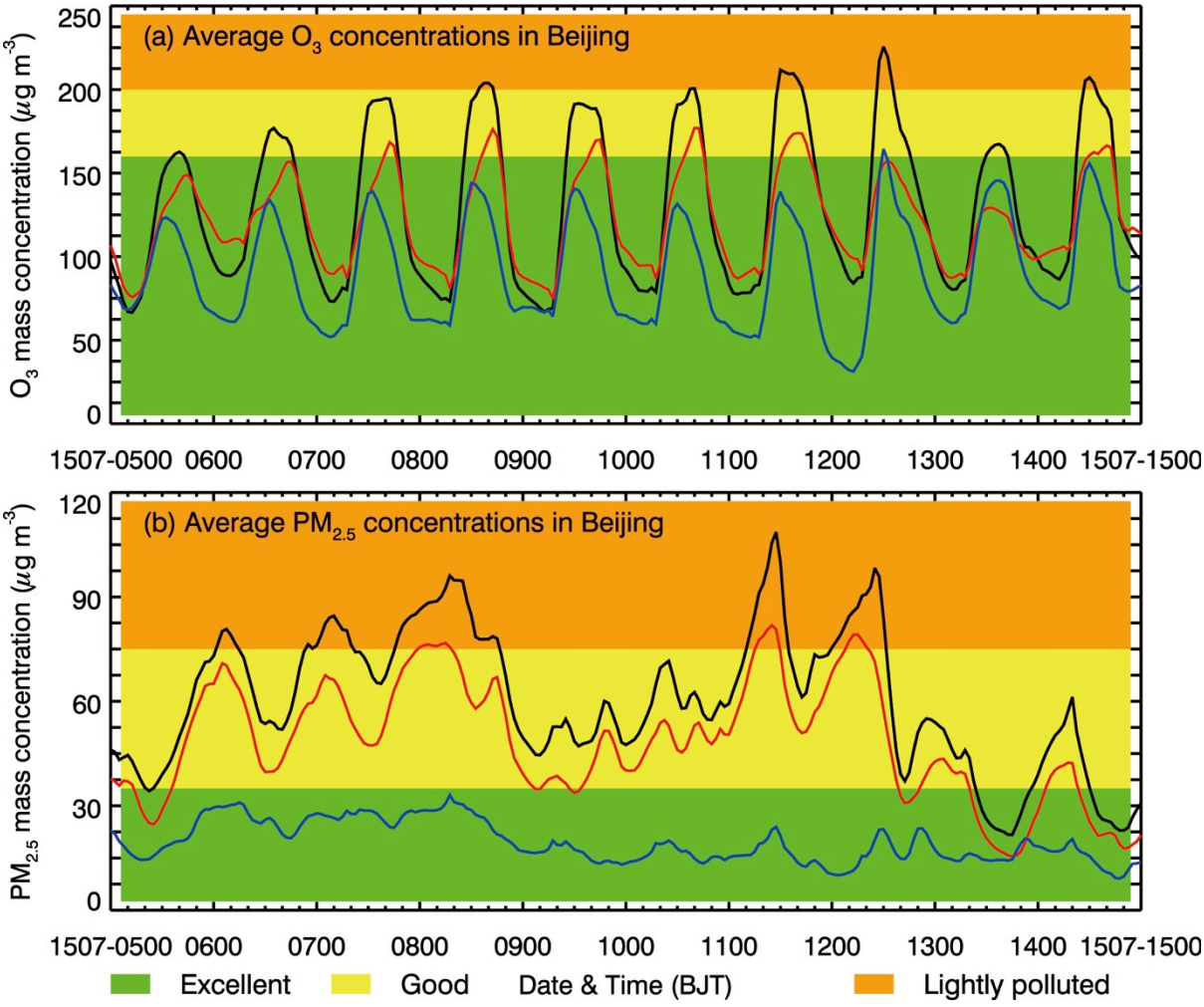
(a) Average O_3 concentrations in Beijing
O_3 mass concentration (μg m^{-3})
250
200
150
100
50
0
1507-0500 0600 0700 0800 0900 1000 1100 1200 1300 1400 1507-1500
(b) Average $PM_{2.5}$ concentrations in Beijing
$PM_{2.5}$ mass concentration (μg m^{-3})
120
90
60
30
0
1507-0500 0600 0700 0800 0900 1000 1100 1200 1300 1400 1507-1500
Excellent
Good
Date & Time (BJT)
Lightly polluted

Figure 10

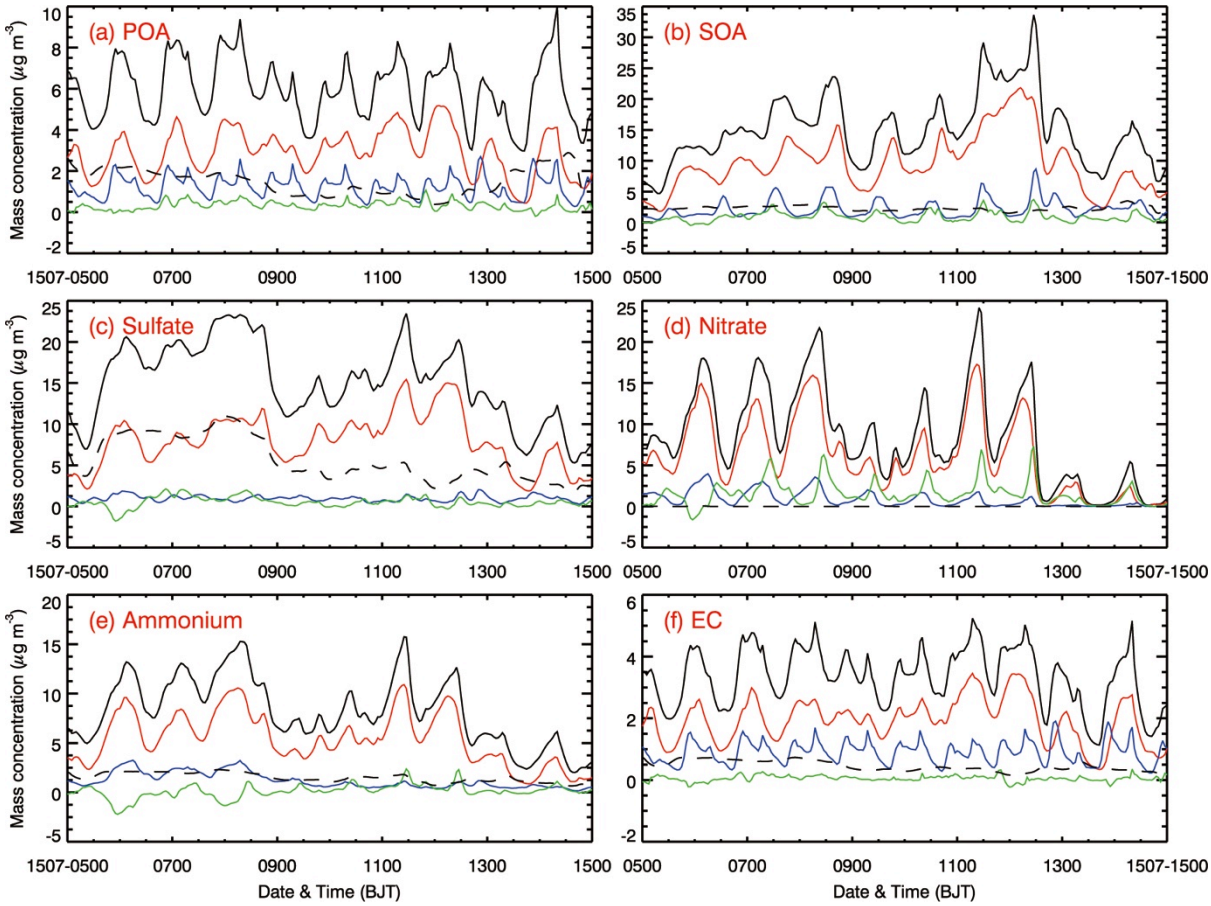
(a) POA
(b) SOA
(c) Sulfate
(d) Nitrate
(e) Ammonium
(f) EC
Mass concentration (μg m-3)
1507-0500
0700
0900
1100
1300
1500
0500
1507-1500
Date & Time (BJT)

Figure 11